DESIGN OF PLASMID AMPLIFIED DNA BUILDING BLOCK SYNTHESIS SYSTEM AND EVALUATION OF DENDRIMER-LIKE DNA FLUORESCENT NANOBARCODES

A Thesis

Presented to the Faculty of the Graduate School

of Cornell University

in Partial Fulfillment of the Requirements for the Degree of

Master of Science

by

Yen Thi Hong Cu

August 2005

ABSTRACT

Methods for producing DNA building blocks with high purity and yield were investigated, including solid-phase DNA synthesis and plasmid amplified DNA synthesis (PADS). In addition, an analysis of the properties of dendrimer-like DNA (DL-DNA) as nanobiosensor was conducted to explore the viability of its real-world application.

Four-armed dsDNA building blocks (X-DNA's) were successfully acquired using solid-phase synthesis. X-DNA consisted of 4 oligonucleotides that are partially complementary such that a cross-shaped dsDNA molecule is formed upon annealing. It was ligated to a 30bp dsDNA spacer immobilized onto micrometer-sized 6% cross-linked agarose beads via biotin-avidin interactions. A subsequent washing step was performed to rid the sample of non-X-DNA structures, and X-DNA was released from the spacer by restriction enzyme digestion. Gel electrophoresis of the product showed higher purity, 72% compared to 67.5% shown in the solution-hybridized X-DNA prior to solid-phase. Characterization of X-DNA was performed by ligation of 4 complementary hairpin loops which serve to close off all open dsDNA ends and prevent the structure from exonuclease digestion. Unchanged DNA concentration after 15 and 30 min of ExoIII digestion at 37^{o}C was observed, confirming the synthesis of X-DNA.

Plasmid amplified DNA synthesis takes advantage of the natural DNA producing system in *Escherichia coli* for high-yield production of plasmids containing sequence for three-armed DNA building blocks (Y-DNA). A nicking enzyme was used to produce a single-stranded break in the plasmid. ExoIII digestion at 37^{o}C was performed to produce ssDNA plasmids. Annealing at 70^{o}C causes a branched hairpin (Y-shape) to form on each ssDNA strand.

Simultaneous digestion of the Y-shape hairpin by three enzymes produces Y-DNA. Single and combinational of enzyme digestion was applied to characterize the ssDNA plasmid, and determined to be a Y-shape structure.

Lastly, fluorescent DNA nanobarcodes were analyzed for their purity, coding capability, compared to concentration-based coding method, as well as differential bleaching of green (G) and red (R) fluorescence. Pure populations of DNA nanobarcodes (4G1R, 2G1R, 1G1R, 1G2R, 1G4R) and multi-code mixtures, immobilized on 5.5um polystyrene beads, were obtained. The fluorescent intensities (R and G) were measured from 12-bit images taken by a wide-field microscope; the illumination source is a Mercury arc lamp and respective fluorescent colors obtained using green and far-red filters. The purity of each population was assessed by analyzing the magnitude of R/G fluorescent ratio standard deviation for each pure barcode populations (N>50beads). Comparison of the mean for each codes to a theoretical R/G ratio yield their codability. The DNA nanobarcodes were determined to be pure and their experimental R/G ratios conform to theoretical values, unlike concentration-based DNA barcodes. Bleaching analysis of red and green fluorodyes reveal that red dye bleach faster than green, however the ratio of R/G, and nanobarcodes, did not change significantly over time.

BIOGRAPHICAL SKETCH

Yen Thi Hong Cu was born in Hanoi, Vietnam and moved shortly after beginning middle school to the Asian Institute of Technology in Pathum Thani, Thailand with her family, where she was first introduced to the English and Thai language, traffic jams, and spicy food. She completed her secondary school work at the Ekamai International School in Bangkok, Thailand in June 1999. Following her graduation, Yen enrolled at Marymount College, Palos Verdes, California and received a degree of Associate of Science in June 2001.

With a desire to study biological phenomena with the hands-on approach of the engineering discipline, Yen transferred to Cornell University into the Biological and Environmental Engineering (BEE) Department as a junior in the Fall of 2001. During her undergraduate career, Yen was involved in several teaching and research experiences, all of which have helped hone her desire to engage in a career in academia. Specifically, her involvement in the study of Nucleic Acid Engineering at the Molecular Bioengineering Lab (MOLBEL) at BEE, conducted in the senior year, spurred her onto the attainment of a Master of Science degree on the same subject.

Yen will remain in the northeastern United States to continue her advanced graduate study in the field of Biomedical Engineering after the completion of her Master degree.

ACKNOWLEDGEMENTS

I would like to thank Prof. Dan Luo for his support and guidance throughout my academic career, and contagious enthusiasm for the pursuit of knowledge. Also, thank you to Dr. Warren Zipfel, Committee member, for his valuable comments and support. I would like to further extend my thanks to Prof. James A. Bartsch and Dr. Ken Zanca, whose academic and moral supports in my undergraduate and graduate years have helped me to both set and achieve my goals.

I would like to extend my deepest and most sincere thanks to my parents, Cu Huy Giai and Nguyen Thi Kim Oanh, for their unending support, love, and belief in my ability to stand on my own two feet. I am grateful for the examples they have set, which I seek to follow on my own academic and personal journey.

Big thank you and hug to my fellow graduate students and the wonderful staff members at Riley Robb, for all the non-academic fun that I could ever have asked for and much more. Your friendly faces makes being at Riley Robb feel more like home each day. Last but not least, I would like to thank all my lab mates at MOLBEL for their supports and inputs that are helpful to the completion of my thesis, and for an enjoyable, unique and enlightening working experience.

TABLE OF CONTENTS

LIST OF TABLES

LIST OF FIGURES

CHAPTER ONE
INTRODUCTION

The recent decade has been the venue of exciting discoveries of nano and micro-scaled materials, such as Quantum dots, metallic nanocrystals, and carbon nanotubes. (Chan and Nie 1998; Endo, Hayashi et al. 2004; Medintz, Uyeda et al. 2005) The scientific community thus finds itself empowered to delve deeper into the exploration of environmental, biological, and biomedical phenomena in dimensions smaller than the tip of a pin—a vision put forth by notable scientist R. Feynman in 1959, when the possibility of carrying out such experiments were still far away. With these new found tools, it has become necessary for material scientists to create biomaterials of equally small size that can be incorporated efficiently with accuracy and specificity, forming functional nanosystems that can then be used for myriad applications in scientific research. Also, due to the small dimensions, many are turning to the bottom-up approach of fabrication, where supramolecular structures are built from controlled assembly of smaller, basic entities in a fashion much like molecular Lego.

These “building blocks” include single molecules or atoms, carbon nanotubes, fluorescent Quantum dots or single dyes, various proteins and antibodies, and nucleic acids. Unlike its predecessor, the top-down approach (i.e., lithographic and electron beam etching methods that strip down complex substrate to form desired structure) is not limited by instrumentation, which confines the size of features to 100nm+ with variable uniformity. The bottom-up approach is the way of the future in nanofabrication, yielding smaller and more precise structures due to the specificity in assembly of its constituents. (Niemeyer 1999; Zhang 2003)

In the past decade, a movement has been initiated to synthesize or uncover new building blocks that can be made abundant, are stable, and contain capability of self-assembly for nanofabrication. Surprisingly, molecular biology was the answer to this need. Amino acids, fatty acids, sugars and nucleic acids are all monomers which are found in great numbers in nature with the ability to aggregate into complex structures, to form the fabric upon which life is built. Among these, molecules with ability to form specific bonds are amino acids (antibodies, transcription factors, etc.), and nucleic acids (RNA and DNA). (Luo 2003) Though diverse in terms of size and ligands, protein recognition and folding patterns are more difficult to predict than nucleic acid's. (Whitesides, Mathias et al. 1991) Traditionally used to store and convey genetic messages, nucleic acids contain 4 monomers (vs ~21 amino acids), are nano-scaled, can form 2D and 3D structures (e.g., double helix, Holliday junctions, tRNA) and are structurally conservative and chemically stable. The challenge, then, is to adapt this biological molecule for fabrication purposes.

Due to its higher stability and more predictable folding pattern, DNA is the material of choice for making nucleic acid building blocks. Several examples of DNA building blocks that self-assembled into supramolecular structures such as arrays, patterns or nano "machines" have been explored, which will be discussed in greater detail later in the text. These efforts form the stepping stone for the development of nucleic acids for generic, not genetic purposes (Luo 2003; Li, Tseng et al. 2004), which will undoubtedly be a large force in advancement of nanofabrication.

1.1 Physical and Chemical Properties of DNA

DNA, properly known as deoxyribonucleic acid, was discovered in 1868 by Friedrich Miescher, a Swiss biologist, but its structure was not deciphered until 1953 by Watson and Crick (Bloomfield 2000). The DNA molecule is composed of an alternating ribose and phosphate backbone, and 4 branching acid bases: adenine (A), thymine (T), guanine (G), and cytosine (C), which make up the core of the DNA molecule. The bases from a single strand pair with another of a different strand via specific H-bonding (purine:pyrimidine; A with T, C with G). The backbone encircles outward, while the bases at the core of the molecule stack upon their neighbors via flat sides, in a slight rotation from the central axis which results in the famous double helical structure of DNA. Depending on the sequence of bases, DNA binding molecules and concentration of ions (e.g., Na+), the DNA double helix can take on different conformations such as the B form (more common, right-handed and extended), A form (shorter and wider, found in dehydrated solutions) and Z form (left-handed and extended, occurring in sequences with alternating purines and pyrimidines) (Table 1.1) (Bustamante, Bryant et al. 2003)

Table 1.1 DNA Double Helix Forms and Dimensions

	A	B	Z	Z (WC)
Handed-ness	Right	Right	Left	Left
Diameter	26	20	18	--
bp tilt	20^{o}	6^{o}	7^{o}	--
bp/turn	11	10	12	12
Rise/bp	2.9	3.4	-3.9 (CpG) -3.5 (GpC)	-3.9 (CpG) -3.5 (GpC)
Helix pitch	32	34	45	45
Helix twist	32.7	36	-10, -50	-68, +8
MG depth/width	13.5 2.7	8.5 11.7	Convex	Flat
mG depth/width	2.8 11	7.5 5.7	9 4	Deep Narrow

A number of parameters are used to define the physical properties of the DNA molecule. Due to the different number of hydrogen bonds in each purine:pyrimidine pairs (A=T, C≡G), the binding energies of each double stranded DNA (dsDNA) molecule varies, as does its melting temperature, Tm. Tm is considered when forming dsDNA building blocks from oligonucleotides, which must first be completely denatured and slowly annealed over an optimized time period (see Chapter 2) and is dependent on the buffer compostion (e.g., [Na+]), pH of solution, where ssDNA is favored due to the protonation of bases, solvents that destabilize DNA's ordered form (e.g., methanol, Formamide, urea), and GC content of a sequence. Variations of formulas calculating Tm can be found. For perfectly paired dsDNA, $Tm(^oC) = 193.67 – (3.09 – Fcg)(34.64 – 6.52\log[Na+]$ where Fcg is the fraction of CG in the entire sequence. Considering effect of duplex length, D, and percentage of mismatches, P, but neglecting effect of GC content, the equation is modified as follow: $Tm(^oC) = 81.5 + 41\ Fcg + 16.6\log([NA+]/(1.0+0.7[NA+])) – 500/D – P$. (Bloomfield 2000)

Each dsDNA also possess a specific ΔG, as a result of free energy given off by H-bonding of bases that is established on the nearest neighbor model (Whitesides, Mathias et al. 1991; SantaLucia 1998). This is considered when determining the folded conformations of ssDNA's, where the lowest ΔG is projected to yield the major product. Though the double helical structure is most prevalent, non-Watson-Crick base pairing such as Hoogstein is also possible. This triple base pairing occurs when one base becomes protonated and forms H-bond with two other bases. Quadruplex (or tetraplex) DNA occurs readily in G-rich sequences, with and the two pairs of helices adopting either parallel or antiparallel directions. However, these forms are induced only at

specific conditions, and Watson-Crick base paring is generally expected in physiological and environments. (Bloomfield 2000; Nelson 2000)

With its origin as a genetic information carrier, DNA is physically stable and resistant to mutations. Moreover, a multitude of enzymes are available in nature that make, bind to, or modify DNA; such as DNA ligase which covalently links DNA phosphate backbones, endonucleases that specifically or indiscriminating cleave dsDNA, exonucleases that degrade DNA from their open ends, or enzymes that provide modifications like phosphatases that covalently add a phosphate group at 5'end of DNA chain or topoisomerases that alter the topography of circular DNA (Luo 2003).

A common way to quantify DNA molecules is by measuring its absorbance at 260nm, where dsDNA has a lower absorbance due to H-bonding and base-stacking interactions that inhibit energy absorption, than ssDNA (Bustamante, Bryant et al. 2003). Two physical parameters, Twist (Tw)—the number of helical turns along the molecule, and Writhe (Wr)—measures the coiling of DNA helix about itself, are used to describe DNA, particularly in dsDNA supercoiling, which is commonly found in DNA packaging and circular bacterial plasmid DNAs. The degree of supercoiling (σ) is defined as $\sigma = (Lk - Lko)/Lko$, where Lk is the linking number ($Lk = Tw + Wr$), and Lko is the number bases / bases per turn. (Strick, Allemand et al. 2000)

At a glance, the DNA double helix is a nanoscale cylinder with a diameter of 2nm, helical pitch 3.4-3.6nm and vertical distance between bases of 0.34nm (Bloomfield 2000) Though seemingly simple in structure, the DNA molecule is one of rather interesting chemical and physical properties. Despite its small diameter, the DNA double helix is a remarkably stiff molecule that

possesses a persistence length of 150bp (50nm at 25^{o}C, 0.2M ionic strength), and a torsional persistence length—the distance between bases below which there is no response to twisting force—of ~180bp. This stiffness is hypothesized to be the result of base stacking interactions and the charge repulsions between the negative phosphate groups that lines the exterior of the helix. (Williams and Maher 2000; Bustamante, Bryant et al. 2003) A previous study has verified DNA to be elastic. Using optical tweezers, researchers stretched ssDNA and dsDNA to ~95% of contour length. It was observed that ssDNA extension per bp is shorter than dsDNA for a tensile force <6pN but the reverse is true for >6pN. A different study showed dsDNA extended at ~3pN forms stretched, positively overwound Pauling DNA (PDNA) that resemble an inside-out helix, which has 2.6bp/turn and roughly 5 times smaller in diameter than normal B-form DNA (Allemand, Bensimon et al. 1998) Mechanical unzipping of bacteriophage (lambda phage) dsDNA indicates that a force of 12pN is required to separate AT rich regions, and 15pN for GC rich regions. (Essevaz-Roulet, Bockelmann et al. 1997)

By its physical properties, such as nanoscale size, stability, rigidity, and specificity in assembly, DNA is suitable material for building supramolecular structures from the bottom up. In addition, various biological “tools” are available for DNA modification prior to, during, or post assembly, making it a specific yet versatile material.

1.2 DNA Building Blocks

As one must probably have discerned at this point, DNA building blocks that are used to build supramolecular structures must have more “branching sites” than a simple double helix, or linear dsDNA. Branched DNA structures are, in fact, found in nature, such as the Y-shaped replication fork and X-

shaped Holiday junction, both transient and unsuitable for engineering purposes. In most cases where DNA is used to form larger structures, Y and X shaped DNA's, with valency of 3 and 4 respectively, are utilized as basic building blocks. Great care is taken in the design of the oligonucleotide sequences that constitute these structures. They are summarized into a number of basic guidelines listed as follows:

1. Free energy (ΔG) is calculated for a sequence; a lower free energy is desired. However, intermediate-low ΔG can also be considered.
2. The secondary structure of the molecule is considered. In general, the least amount of secondary structure is desired.
3. The dimerization, triplexation (and even Z-DNA) are considered. The molecules should not form a self-dime, a triplex, or a type of DNA other than the desired formation (A, B, or Z.)
4. The length is considered. It should be long enough to form a stable DNA structure (at least more than 8 nucleotides (nt) long).
5. The helix geometry is considered. Half-turns are the quantum of the design (5*n bp, where n = 0, 1, 2... are between junctions).
6. The G/C content is considered. In general (varies by design), sequences are routinely chosen that constitute about 50% G/C.
7. The symmetry is considered. Sequence symmetry (e.g., as those occurred in Holliday Junctions) of each arm should be avoided.
8. Non Watson-Crick base paring is considered. Sequences containing more than 2 consecutive G's should be avoided.
9. For X-DNA it is recommended to design complementary segments/arms that are longer than 15 nucleotides.

   The actual sequence of the starting oligonucleotides is determined

following the above guidelines, and using sequence symmetry minimization. This can be done simply by hand or using an algorithm developed by Seeman (Seeman 1990). Programs (e.g., NANEEV) that design the optimum sequences based on their ∆G once folded has been developed, but have not presently been found to be a popular method. In addition, a previous study has shown that [Na+] inversely affect the stringency, f, in DNA hairpin hybridization by the following formula: $f = \exp(-\Delta G/RT)$, where ∆G is the free energy of matching vs. mismatching sequences.(Broude 2002) Therefore, [Na+] must be kept at minimum during annealing procedure to ensure high fidelity in formation of the intended DNA building block.

The dimensions of most structures are well under dsDNA persistence length of 50nm so that their tertiary structures are more defined. 2D structures are relatively easier to characterize than 3D, though some indirect evidence of their formation have been proven by gel electrophoresis (Seeman 2003; Seeman 2005). The junctions between arms of Y-DNA was shown to be flexible (Ma, Kallenbach et al. 1986), and similar finding was shown in a later study of DX-DNA junction (Sa-Ardyen, Vologodskii et al. 2003). However, it is believed that formation of supramolecular structures such as arrays or dendrimers help stabilize these building blocks and confine them to a certain regular conformation. (Winfree, Liu et al. 1998; Mao 1999; Sha, Liu et al. 2000; Yan 2003; Li, Tseng et al. 2004)

1.3 Synthesis of DNA Building Blocks and Supramolecular Structures

DNA oligonucleotides are commercially available through suppliers such as IDTDNA or Fisher Scientific. Immobilized on a solid support, DNA bases (A, T, C, or G) are added one by one to a growing strand to yield a sequence as specified by the user. The costs of these products vary by their

length, expected yield, purity (i.e., desalting, PAGE, or HPLC purifications) and chemical modifications (i.e., phosphorylation, biotinylation, fluorophore conjugations). The average price for oligonucleotides varies by the synthesis scale as well as purification method. Added costs include phosphorylation and/or modifications of 5' or 3' ends of the molecule (see Tables 1.2, 1.3).

Following ssDNA synthesis, the oligonucleotides must be annealed to form the DNA building block structure. The annealing process can occur in step-wise (adding one oligonucleotide at a time) or one-pot approach, and must be optimized in terms of annealing temperature, buffer ionic strength, and time—which may range from 30min (Li, Tseng et al. 2004) to 2 days (Yan 2003; Sa-Ardyen, Jonoska et al. 2004) This added step introduces a new variable that further reduces the yield and purity of building block DNA's, where incompletely annealed may be present in the solution.

Purity is imperative in establishing DNA as a viable biomaterial. One method to obtain pure DNA building block is through solid-phase synthesis (Chapter 2) where pure X-DNA is produced from a solid support. The cost and yield in production of DNA building blocks is another important factor. A new way to synthesize Y-DNA that takes advantage of the natural DNA producing capability of living organisms was explored. *Escherichia coli*, more commonly known as *E. coli*, is a bacteria that is used extensively for genetic cloning purposes. The bacteria houses and replicates circular dsDNA molecules called plasmids, which originally serves as carrier of genetic information vital for the bacteria's adaptation and evolution in its ever changing environment.

Table 1.2 IDTDNA Custom Oligo Pricing*

Synthesis Scale (µmole)	Price ($/base)	Lengths (bases)	Guaranteed Yield** (O.D.)	PAGE	HPLC	IE HPLC	RNase-Free HPLC	Dual HPLC	Dual PAGE & HPLC
0.025	$0.35	15-45	3	N.A.	N.A.	N.A.	N.A.	N.A.	N.A.
0.1	$0.55	10-80	6	$40	$40	$40	$70	$75	$85
0.25	$0.95	5-100	15	$60	$60	$60	$85	$115	$125
1	$1.95	5-100	45	$125	$100	$115	$140	$215	$230
10	$18	N.A.	N.A.	$900	$350	$425	$560	$860	$137

Table 1.2 (Continued).

Synthesis Scale (µmole)	PAGE Purification (O.D.)	HPLC Purification (O.D.)	IE-HPLC Purification (O.D.)	RNase-Free Purification HPLC (O.D.)	Dual HPLC Purification (O.D.)	Dual PAGE & HPLC Purification (O.D.)
0.025	N.A.	N.A.	N.A.	N.A.	N.A.	N.A.
0.35	1	1	1	1	1	0.5
0.55	2	4	4	4	2	1
0.95	10	20	20	20	10	5
1.95	N.A.	N.A.	N.A.	N.A.	N.A.	N.A.

*Price as listed from July 25, 2005 on www.idtdna.com
**Yields (listed for unmodified oligos 20-100 bases in length)

Table 1.3 Fisher Oligos (Sigma Genosys) Oligo Pricing*

Synthesis and Purification Pricing					Guaranteed Yields**			
Synthesis Scale (µmole)	Desalted ($/base)	Cartridge Purified ($/oligo)	PAGE ($/oligo)	HPLC ($/oligo)	Desalted Purified (O.D./µg)	Cartridge Purified (O.D./µg)	HPLC Purified (O.D./µg)	PAGE Purified (O.D./µg)
0.025	0.30	N/A	N/A	N/A	N.A.	N.A.	N.A.	N.A.
0.05	0.75	25.75	77.25	77.25	5/150	1/30	1/31	0.5/15
0.2	1.30	25.75	77.25	77.25	12/360	3/90	2.5/75	1/30
1	2.25	41.20	113.30	113.30	40/1200	12/360	13/390	5/150
10	20.60	N.A.	N.A.	190.55	400/12000	N.A.	130/3900	N.A.
15	N.A.	N.A.	N.A.	N.A.	600/18000	N.A.	190/5700	N.A.

* Prices as listed on July 25, 2005 on www.fisheroligos.com
** Guaranteed is for 20-mers or longer; shorter oligomers will have proportionally fewer O.D.s. Modified oligos will typically be 40% of the above stated yields.

Plasmids can range from 4.5-9kb (non-conjugative plasmids) to 37-120kb (conjugative plasmids) and copy number varies per bacterium depending upon the type of plasmid and its origin of replication. (Smith-Keary 1989) In the lab, the plasmid is engineered to enable the insertion of a specific sequence that needs to be amplified. Lab strains of E. coli have been developed to efficiently produce engineered plasmid DNA's with high fidelity, a trait that is key in production of pure DNA building blocks.

DNA building blocks are radically different from linear DNA, in that they contain high secondary structures such as hairpin loops (called inverted repeat (IR) sequences in bacteria) and cruciform structures (4 hairpins). Under physiological conditions, they can be found near origins of replications, operator sequences, transcription termination regions, insertion sequences and transposons of the *E. coli* genomic and plasmid DNA, and thus has implied functional significance. (Mizuuchi 1982; Smith-Keary 1989) A naturally occurring palindromic (hairpin) sequence that is viable in bacteria could be as long as 66bp (in the *lac* operator sequence). However, a study that introduced fully palindromic plasmid DNA (pBR322, 4.36kb) into *E. coli* N100 *recA* found that the bacteria failed to replicate and maintain this structure.(Mizuuchi 1982)

There is a possibility that the high secondary structure may induce mutation during DNA replication such as deletions (skipping over of hairpin), or recombinant mutations due to palindromic sequences. A protein important in recombinant repair of *E. coli* is the *recA* protein, which binds to ssDNA and promotes homologous pairing during the formation of the Holliday junction. (Smith-Keary 1989)) Building block sequences have a high secondary structure and can form Holliday junctions, which lead to recombinant of DNA. Thus, it is important to discourage recombinant repair mechanism in *E. coli*

host strain such as TOP10, a DH10B™ derivative strain, which has a mutated form of *recA* (*recA1*).[1]

In an effort to produce Y-DNA at high number, sequence for one (or several) DNA building block can be encoded in a plasmid to be cloned. Extraction of these structural forms can be achieved by conversion of dsDNA to ssDNA and released with specific restriction enzyme digestion (see Chapter 3). To date, no other efforts that involve producing DNA building blocks directly from *E. coli* plasmid have been realized. Using bacteria to DNA, in theory, guarantees fidelity in DNA replication and simultaneously reduces the cost of production. It is, however, time consuming and the possible difficulty in bacteria replication of hairpin loops are some factors that must be considered.

1.4 Nanobiotechnology and DNA

The recent advancements in nucleic acid engineering for generic purposes have paved a new frontier in the field of nanobiotechnology. The physical properties of nucleic acids: structural stability, stiffness, and small size, combined with the chemical ability of self-assembly by specific base-pairing and the availability of various nucleic acid modifying enzymes, makes the possibility of using nucleic acids for bottom-up fabrication a real and nearing future. Nucleic acids such as DNA and RNA have branched out from their traditional role as carriers of genetic information, and have been proven to be a viable nano-scale self-assembling material from various designed building blocks in the bottom-up approach (Seeman 1998; Luo 2003; Seeman

---

[1] TOP10 genotype: F^- *mcr*A Δ(*mrr-hsd*RMS-*mcr*BC) ϕ80*lac*ZΔM15 Δ*lac*X74 *rec*A1 *ara*Δ139 Δ(*ara-leu*)7697 *gal*U *gal*K *rps*L (Str^R) *end*A1 *nup*G. *endA1* for cleaner preparations of DNA and better results in downstream applications due to the elimination of non-specific digestion by Endonuclease I. *recA1* for reduced occurrence of non-specific recombination in cloned DNA (Invitrogen™ technical resource).

2005), which has numerous potential applications from scaffolding for crystallography, template for nanoscale patterning, computing, to nanomechanical machines.

Efforts to utilize DNA as biomaterial were pioneered 10 years ago by Nadrian Seeman, whose research, starting from immobile Holiday junctions whose arms contain nonidentical sequences, went on to design stable 3, 4, 5 and 6-branched DNA molecules (Kallenbach 1983; Seeman 1990; Wang, Mueller et al. 1991), 3-D DNA structures such as cubic and concatenated DNA circles (Borromean rings)(Chen and Seeman 1991; Mao, Sun et al. 1997)(Figure 1.1), as well as double-crossover (DX) and triple-crossover (TX) DNA's (Figure 1.2) that could be assembled into regular crystalline arrays.(Fu and Seeman 1993; Winfree, Liu et al. 1998; LaBean 2000) Since then, the specificity in assembly and versatility in application of DNA as a material and device has been explored by several research groups. Though it is not possible to list every single example, I will try to highlight a few prominent studies of DNA, particularly those that explore the programmable self-assembly of DNA into unique structures and scaffolds, which will help shed light onto the current progress as well as the future direction of the field of nucleic acid engineering.

DNA application in building regular 2-D or 3-D arrays was initially proposed for applications in X-ray crystallography by N. Seeman, where the array is used as a scaffold for organic molecules such as proteins. (Seeman 1982) And indeed, a number of 2-D arrays of DX and TX DNA's have been synthesized with different basic shapes (rectangles, rhombuses, or pseudo hexagons).(Mao 1999; Mao, LaBean et al. 2000; Ding, Sha et al. 2004)

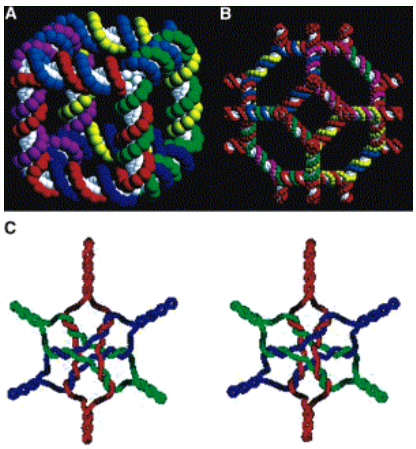

Figure 1.1 DNA Cube and Borromean Ring(Seeman 2003)

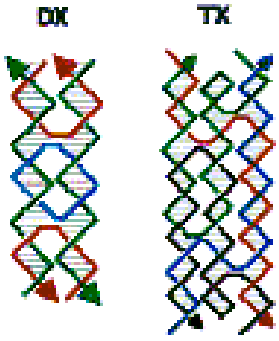

Figure 1.2 Double-Crossover (DX) and Triple-Crossover (TX) DNA(Seeman 2003)

A recent demonstration of this concept was done by Yan et al who constructed 4-armed DX DNA building blocks, each of which consist of 9 oligonucleotides. Each tile possess an inherent curvature, thus by controlling their orientation and order relative to each other, it is possible to form regular flat arrays (alternating concave by convex) or conductive DNA ribbons (concave by concave) structures that are ~35nm in diameter after silver metallization. Each 4 x 4 tile contain a biotin molecule at the center, and when the array was subsequently introduced to streptavidin, a tetramic protein that bind tightly to biotin, a regular pattern of streptavidin on the array was detected

by AFM. This finding affirms the possibility of using DNA arrays for X-ray crystallography. (Yan 2003)

DNA self-assembly is not limited to 2-D arrays but also extends to 3-D as well. One approach is to form building blocks for an array with inherent curvatures, so that the resulting array would arc and eventually close to form a tube after ligation (Yan 2003). Other tubular structures have also been formed using specially designed oligonucleotides. Mathieu et al successfully constructed a hexagon symmetric DNA tube that consists of 6 double helices joined together by DX DNA. The tubes are less than 15μm in length and roughly 6nm in diameter (middle opening is about 2nm wide, the size of 1 double helix). They contain sticky ends on the side, such that when ligated together could form a 2D array of side-by-side tubes (Figure 1.3). The authors propose to utilize these structures as nanomechanical struts due to its stiffness. The neutral outer and inner surfaces of the tube may lead to application in encapsulation of carbon nanotubes (for ease in surface modifications) or impaling of cells for the delivery of foreign substances. (Mathieu, Liao et al. 2005)

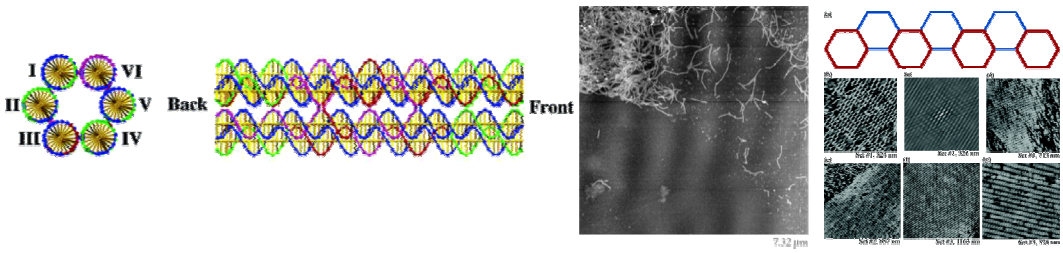

Figure 1.3 6-Bundle Helical DNA as Tube and Flat Array

3D structures could also be constructed by putting together “tiles” of TX DNA, as shown by Liu et al. Two different sets of TX-DNA tiles, A and B, were made. Unmodified, these flat tiles assemble via sticky end programming (A-B-A) into a flat 2D DNA array. Upon thiol modification of the B tile, which introduces a curvature in the 3D structure, the assembly of A and B tiles formed DNA nanotubes that are ~25nm in diameter and up to 20μm in length. Silver metallization of these TX DNA result in a smoother and uniform conductive silver nanowire of ~40nm in width. (Liu, Park et al. 2004)

Another example of 3D DNA structure is one that is made from a single oligonucleotide. A recent study by Shih et al introduced a 1.7kb single stranded oligonucleotide could self-anneal into a 3-D octahedron, a geometric solid with 8 planar triangular faces. Of the 12 struts that form the octahedron, 5 were DX DNA and 7 were paranemic crossover (PX) DNA’s, each measure ~14nm. They were joined at 6 4-way junctions. Visuallization of the octahedron under cryo-electron microscope shows uniform structures about 22nm in diameter. The 3-D octahedrons are expected to be rigid structures, and have intended application as carrier of molecules, either by encapsulation or covalent surface modification. (Shih, Quispe et al. 2004)

1.5 DNA as Scaffold for Hybrid Structures

In his presentation to the American Chemical Society in 2000, C. Mirkin described DNA as a nanoscale bricklayer and “mortar” that could be used to assemble nanoscale building blocks of different materials. (Mirkin 2000) Two early works to demonstrate this concept by Mirkin’s group involve conjugation of DNA to gold (Au) nanoparticles (diameter=8-30nm). In the first experiment, 2 batches of ssDNA (A and B) were immobilized by thiol covalent bonds separately onto 13nm diameter Au particles. By adding a linking

oligonucleotide partially complementary to both conjugated ssDNA's, the Au particles were brought together via a sandwiched complex (A-ssDNA-B). Due to the multivalency of the particles, a network of 13nm Au beads formed so large that it precipitated out of the solution. This is a completely reversible process, by heating and denaturing the DNA complexes. The color change during this reaction was used as an indicator when sensing PCR-amplified DNA from *bacillus anthracis,* where this DNA was used in place of the linking oligonucleotide. (Elghanian, Storhoff et al. 1997)

This work was followed by another study from the same group, where similar sandwiched hybridization models were used with 8nm (A) and 30nm (B) Au beads. Different types of complexes were made by adjusting the concentrations of the beads with DNA as linker, such as network structures, 30nm surrounded by 8nm (A>>B), or vice versa (B>>A), which further demonstrates the ability of DNA for specific assembly of hybrid materials. (Figure 1.4) (Mucic 1998)

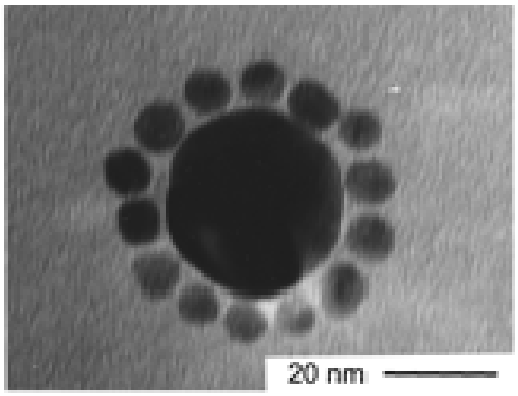

Figure 1.4 DNA-Mediated Assembly of Hybrid Nanogold Particles(Mucic 1998)

Discrete nanostructures were also synthesized by Alivisatos research group. Using DNA as scaffolding, they successfully attached different number of Au nanocrystals onto a central quantum dot (QD) (Fu, Micheel et al. 2004). Oligonucleotide conjugation to QD and Au is as follow: Au conjugated to a single oligonucleotide complexes were purified by gel electrophoresis, and streptavidin coated QD were introduced to biotinylated complementary oligonucleotides. After hybridization, complexes with different number of Au surrounding QD was purified from gel and visualized by TEM. They show to be regular in structure and may have special optical properties or application as nanoprobes. (Figure 1.5)

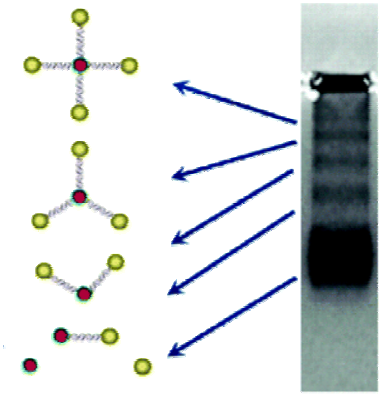

Figure 1.5 DNA-Mediated Assembly of Nanogold Particles and Quantum Dot(Fu, Micheel et al. 2004)

A study in 2003 by Zheng et al showed ssDNA could bind sequence-specifically carbon nanotubes (CNT's) (Zheng, Jagota et al. 2003). Following that, some researches have combined DNA and CNT, such as DNA-templated assembly of CNT's for application in electronic circuits. (Keren, Berman et al. 2003; He and Dai 2004) An example of DNA-directed construction of complexes containing more than one CNT's by hybridization was demonstrated, where single ssDNA bound CNT's were brought together via

hybridization with a multivalent ssDNA-modified Au nanoparticle. (Li, He et al. 2005) The CNT was subjected to acid oxidation to produce a carboxylic group for the grafting of amine-modified ssDNA. The complementary ssDNA sequence was conjugated onto Au nanoparticle by thio-Au chemical linkage. The resulting structure was visualized with AFM, which showed 4 CNT's extending from a junction with a raised Au particle.

DNA directed detection of antigens (e.g., pathogenic anthrax lethal factor DNA) at 500 zeptomolar (10^{-21}M) levels using magnetic microparticles and Au nanoparticles, both conjugated to ssDNA probes (by thiol and SMCC, respectively) was also achieved (Nam, Stoeva et al. 2004). Here, target DNA was separated from the solution using magnetic beads and Au nanoparticles in a sandwich assay under a magnetic field. After washing steps, the target DNA was released by heating of the complex. Confirmation that target DNA was indeed captured by probes was done by a Southern blotting setup. Au nanoparticles and target DNA dissociated from the magnetic microbeads were hybridized onto immobilized capture oligonucleotides cross-linked on a solid surface (Au-targetDNA-oligonucleotide-surface). Subsequent silver metallization of the Au particles confirm the presence of target DNA. The specific hybridization allows distinction of single basepair mismatches, and detection of as little as 10 DNA strands per sample, which is comparable to PCR sensitivity. (Figure 1.6)

Beside nanocrystals, DNA could also be combined with molecules such as fluorophores or phospholipids for nanopatterning on a solid support (Yoshina-Ishii and Boxer 2003) or surface modification of liposomes, possibly for drug delivery. In additions, surface modifications also have been extended to biological materials such as diatoms (Rosi, Thaxton et al. 2004). It must be

noted that all of the above examples shows the ability of DNA to specifically assemble isotropic molecules, in other words, one cannot control the number and type of oligonucleotides that is conjugated to Au nanoparticles, QD, or liposomes. Thus, control of the number ratio as well as relative positions of assembly for these building materials is severely limited.

There is, however, an answer to this roadblock. We do know that DNA building blocks are anisotropic molecules, since the sticky end on each arm can be specially programmed. The logical next step, then, is the marriage of anisotropic DNA building blocks with other these molecules to form anisotropic self-assembling building blocks. A recent publication realized this concept by building anisotropic DL-DNA which holds 2 colors of fluorophores (Green and Red) in a tightly controlled ratio (4G:1R, 2G:1R, 1G:1R, 1G:2R, 1G:4R). (Li, Cu et al. 2005) These complexes, called fluorescent DNA nanobarcodes, also contain a molecular recognition element, in this case an ssDNA probe that recognizes different sequences of viral DNA. In the presence of target (viral) DNA and a solid support (polystyrene bead) that has a partially complementary ssDNA capture sequence, the nanobarcodes are immobilized onto the bead in a sandwich assay similar to the one described above by (Elghanian, Storhoff et al. 1997). This enabled multiplexed detection of up to 3 different viral DNA's in one solution by flow cytometer or fluorescent microscopy. Using a flow cytometer, the detection limit is up to attomolar level and at less than 15 seconds. Its small size (~20nm diameter), stability and biocompatibility make it a powerful tool for multiplexed sensor of reactions or entities *in vitro, in vivo* or in environmental monitoring (Chapter 4).

The DNA nanobarcode is one of the first among the new generation of bottom-up synthesized, nano-scaled anisotropic devices. In preparation for its

real-world application, it is necessary to study the properties of the nanobarcode such as purity, coding capacity, differential dye bleaching, and specificity vs. traditional dye concentration/ encapsulation scheme (see Chapter 4).

1.6 DNA of the Future

DNA has been shown to a material that is versatile yet programmable with high specificity. Its predictable assembly scheme, small size, abundance, availability of modifications and modifying "tools", and stable, rigid structure is a major asset over other molecules (e.g. RNAs, proteins, lipids) in its role as a scaffold or "smart glue" (Mirkin 2000) in nano-scaled bottom-up synthesis. However, like all molecules that assemble by Hydrogen bonds, DNA supramolecular structures are subjected to destruction by high heat, UV radiation, degradation by DNases, found abundant in nature, and various harsh environmental conditions (e.g., caustic solvents). These limitations may be addressed in the experimental design. Efforts to make alternate DNA motifs (substitute DNA bases (Liu, Gao et al. 2003), TNA (Chaput and Szostak 2003), PNA (Lukeman, Mittal et al. 2004), and nylon DNA (Zhu, Lukeman et al. 2003) are on-going and will also hopefully help address this concern. However, little work has been done using these alternate versions compared to DNA, mainly due to their high cost of synthesis and lesser understood mode of assembly.

Not described in depth in this chapter, though equally of importance, are examples of DNA as computation devices to calculate the Hamiltonian pathway (Adleman 1994) or play tic-tac-toe (Stojanovic and Stefanovic 2003), template material for nanoelectronic circuits (Braun, Eichen et al. 1998; Keren, Krueger et al. 2002; Keren, Berman et al. 2003) and nanomechanical DNA

devices (Mao 1999; Simmel, Yurke et al. 2002; Simmel 2002; Yan, Zhang et al. 2002; Seeman 2005). They, along with the previously mentioned examples of DNA structural building blocks, demonstrate the potential of DNA to be a capable and dependable material to facilitate bottom-up synthesis, where nanometer sized molecules or even single atoms are put together one by one to form robust structures and devices of limitless applications.

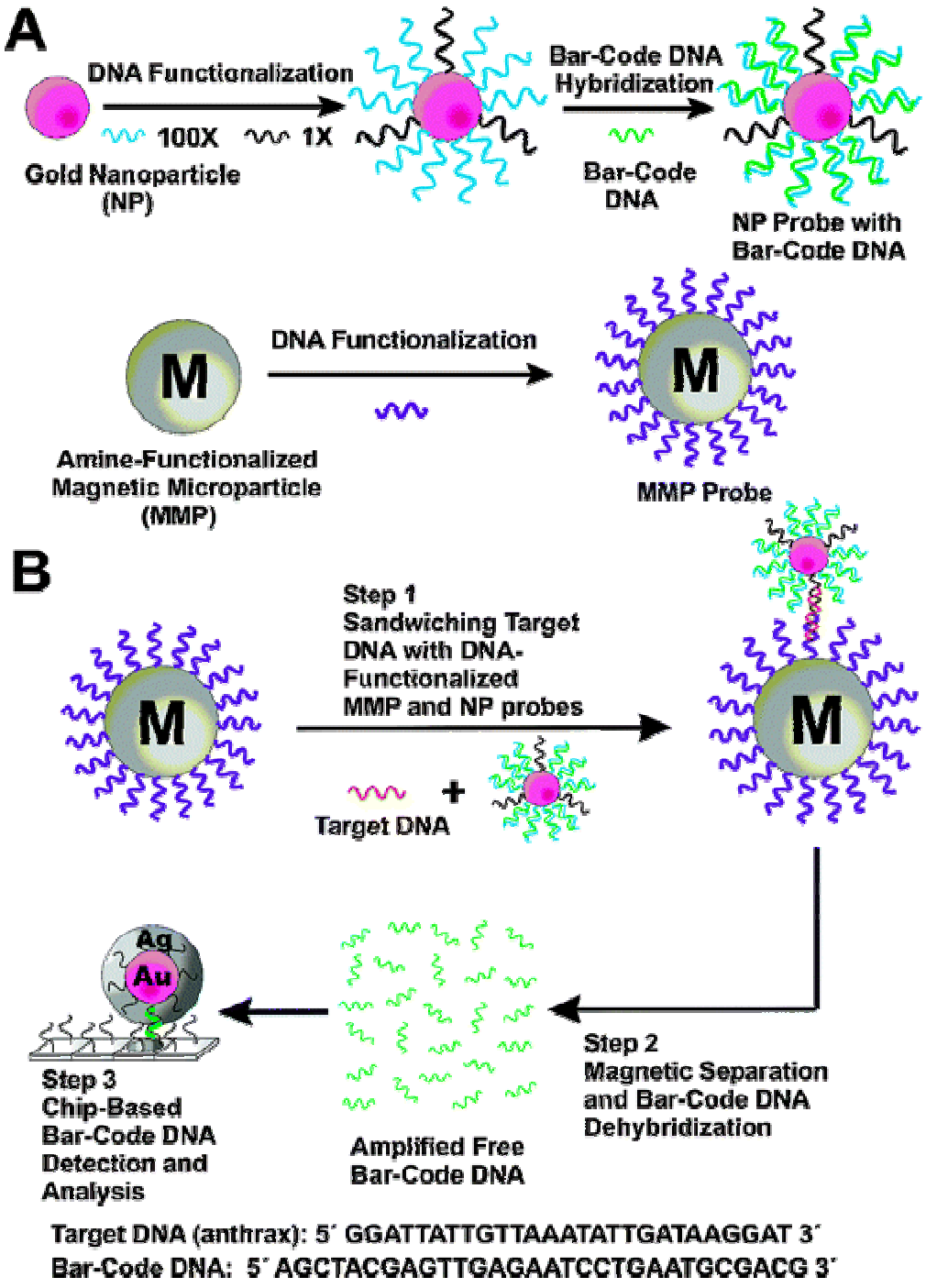

Figure 1.6 DNA Functionalized Nanobarcode(Nam, Stoeva et al. 2004)

CHAPTER 2
X-DNA SOLID PHASE SYNTHESIS

2.1 Introduction and Schematic

Stable, anisotropic, and pure DNA building blocks are important in bottom-up synthesis using DNA as scaffold. In this chapter, I describe the synthesis and characterization of pure X-shaped DNA building blocks in 2 stages: 1) formation of X-DNA in solution and 2) purification of X-DNA by capture on solid support and washing out of impurities (i.e., partially formed structures and mismatching oligonucleotides), followed by X-DNA release by restriction enzyme digestion.

Since two types of X-DNA is present in this scheme, X-DNA after hybridization in solution and X-DNA after release from solid support, for ease of reference, I will call the first X-DNA type “solution phase X-DNA” and the latter “solid phase X-DNA”. Solution phase X-DNA, a tetrameric and tetravalent DNA building block molecule, was formed by hybridization of 4 partially complementary oligonucleotides. (Figure 2.1) The building block contain on (only) one arm a sticky end complementary to a double-stranded spacer DNA molecule that is immobilized onto a cross-linked agarose microbead by biotin-streptavidin interaction. T4 ligase was introduced to ligate, or covalently linking the phosphate backbone, of solution phase X-DNA to spacer DNA. Washing with PBS and ddH_2O eliminates all unbounded (and presumed to be incorrectly formed structures). Digestion of the spacer DNA with Dde1 restriction enzyme releases a new slightly larger “solid phase” X-DNA with all identical arms. (Figure 2.2)

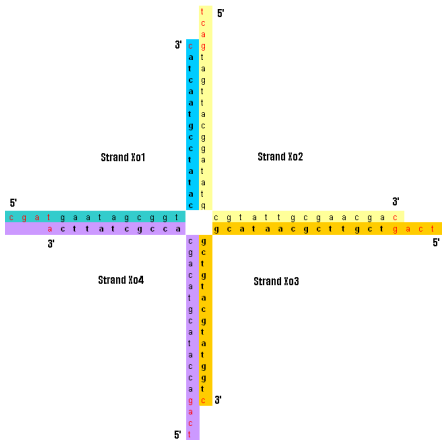

Figure 2.1 Solution Phase X-DNA

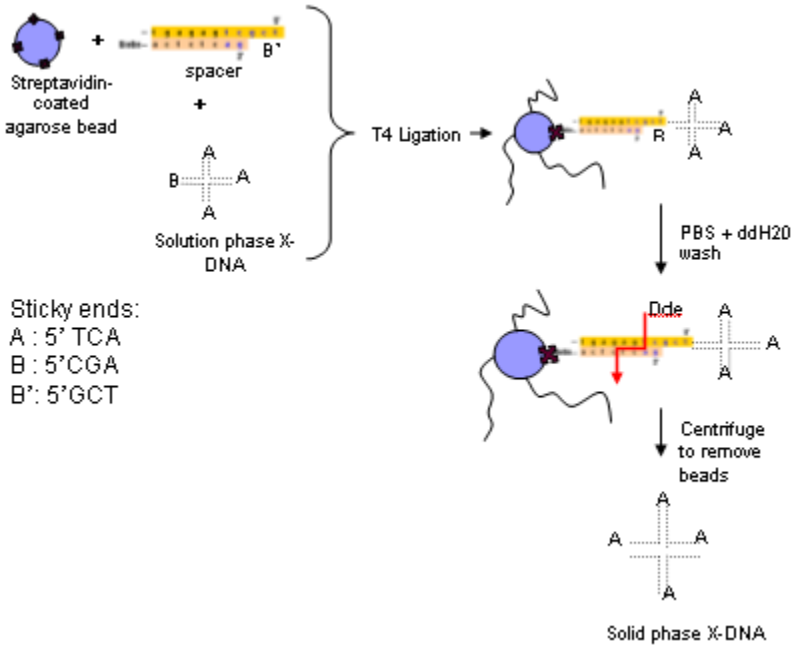

Figure 2.2 Scheme for Solid Phase X-DNA Synthesis

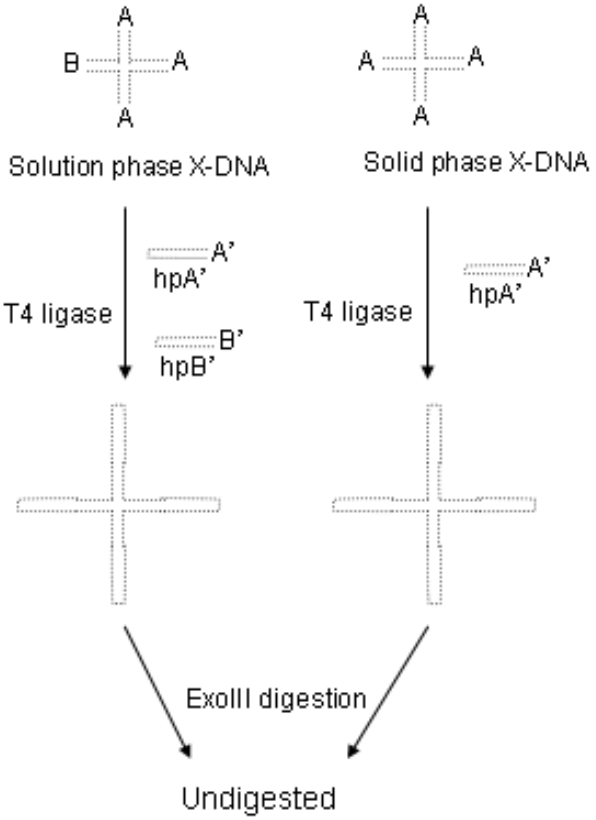

Figure 2.3 Solution and Solid Phase X-DNA Characterization

Characterization of solution phase X-DNA is done using gel electrophoresis. In addition, a new method for characterization of solid phase X-DNA by ligating complementary hairpins to the structure is introduced. Correctly formed X-DNA in solution or solid phase should have a certain molecular weight and contain specific sticky ends. Ligation of 4 complementary hairpins to 4 of X-DNA's sticky ends forms a closed structure that is impervious to ExoIII digestion. Presence of DNA at the correct molecular weight after ExoIII digestion confirms that X-DNA successfully formed. (Figure 2.3)

In this chapter, DNA sequence design and characterization of building blocks is discussed in detail. Also, a brief note on the dynamics in attachment of DNA capture spacers on agarose beads (solid support) via biotin-streptavidin linkage is presented, specifically on the effect of spacer concentration on attachment efficiency.

2.2 Experimental Methods

2.2.1 X-DNA, Spacer DNA, and Hairpin Sequence Design

The DNA sequence design is unquestionably the most important factor in the correct formation of the desired final structure. X-DNA consist of 4 oligonucleotides, named x01, x02, x03, and x04 that are of 29-33nt in length and partially complementary to each other such that they form an X shape when hybridized (Table 2.2.1 and Figure 2.2.1). The rough sequence for each oligonucleotide was designed by the old-fashioned paper and pen method, and further modified to achieve the lowest possible free energy after hybridization of all four oligonucleotides. Empirical criterias for oligo design were considered (see Chapter 1). An additional objective was lower free energy in combinations of strands that are adjacent and supposed to

hybridize: x01+x02, x02+x03, x03+x04, and x04+x01. More importantly, high secondary structures (low free energies) for single oligonucleotides and for combinations of non-adjacent strands (e.g., x01+x03, x02+x04) are avoided. These include self dimmers, hairpin formations, and a series of C/G of more than 4nt's which may cause non-specific pairing or tetraplex formation. Online programs such as m-Fold developed by Michael Zuker[2] and FisherOligos Calculator[3] were used for calculation of free energies. m-Fold was also useful as a "spell checker" since it produces a 2-D schematic of the final secondary structure of the input sequence.

Solution phase X-DNA contain 3 arms that are 15bp in length with A-type sticky ends (5'TCA), and the remaining arm (formed by x01 and x04) only 12bp with B-type sticky end (5'CGA) that is complementary to the DNA spacer. There are two reasons for this AAAB design. Firstly, the unique sequence of the B arm enables immobilization of only 3 possible partial structures: x01/x04, x01/x02/x04, and x01/x03/x04, and X-DNA, instead of 8 possible structures and X-DNA. Secondly, the shorter arm shows to be unstable in solution, which eliminates formation of x01/x04 and helps simplify the purification process. Solid phase X-DNA is released from DNA spacer Dde1 restriction enzyme digestion which leaves the sticky end 5'TCA (type A) at 3bp cut into the spacer (Figure 2.2). This effectively produces an X-DNA molecule that contains 4 identical arms with type A sticky ends. This is an important factor in characterization of X-DNA.

---

2 The Bioinformatics Center at Rensselaer and Wadsworth, DNA and RNA folding applications: http://www.bioinfo.rpi.edu/applications/mfold/

[3] Sigma Genosys oligo calculator: http://www.fisheroligos.com/oligo_calconly.asp

Table 2.1 X-DNA, Spacer DNA and Hairpin Sequence

Structure	Name	Sequence (5'→ 3')	Length (nt)	MW (g/mol)
X-DNA	x01	CGA TGA ATA GCG GTC ATA TCC GTA ACT AC	29	8965.8
	x02	TCA GTA GTT ACG GAT ATG CGT ATT GCG AAC GAC	33	10272.6
	x03	TCA GTC GTT CGC AAT ACG GCT GTA CGT ATG GTC	33	10215.6
	x04	TCA GAC CAT ACG TAC AGC ACC GCT ATT CA	29	8870.7
SpacerDNA	Spacer01	/5BIO/TGC AAT GGC GAT ACA GGT TCA GTC AGG CGA TTA GCA TGT TAC CGT ATA CTC TCA G	55	17371.5
	Spacer02	TCG CTG AGA GTA TAC GGT AAC ATG CTA ATC GCC TGA CTG AAC CTG TAT CGC CAT TGC A	58	17896.6
Hairpins	hpA'	TGA GCA TGC CGT ACT TTT TGT ACG GCA TGC	30	9284
	hpB'	TCG GCA TGC CGT ACT TTT TGT ACG GCA TGC	30	9259.9

Spacer DNA is designed similar to X-DNA oligonucleotides. The first oligonucleotide, Spacer01, contain a biotin molecule at its 5' end, while the second, Spacer02, has phosphorylated 5'TCG sticky end, which is complementary to B arm on solution phase X-DNA (Table 2.1). The spacer length is important in the experimental design, since an excessively short length (e.g., <15bp) may introduce steric hindrance that inhibit attachment of X-DNA onto adjacent spacers, and a longer spacer (e.g. >80bp) has a higher possibility of containing secondary structure which prevents efficient spacer formation. The final design used a spacer 55bp in length.

Design for hairpin used in characterization of solution and solid phase X-DNA was relatively simpler. Two types of hairpins were designed that could anneal to A type sticky end (hairpinA' or hpA') and to B type sticky end (hairpinB' or hpB'). Each hairpins are 30nt's long, with 5 thymines forming the middle loop. Thymine was chosen for this purpose since it is smaller (pyrimidine) and has the lesser number of H-bonds compared to cytosines, which minimizes unwanted secondary structures such as complexing with guanines. All oligonucleotides are phosphorylated at 5' to enable ligation.

2.2.2 Synthesis of X-DNA

Synthesis of solution phase X-DNA was achieved by mixing starting oligonucleotides x01, x02, x03, x04 (stock 0.1mM in 10mM Tris, pH 7.5 - 8.0, 50mM NaCl, 1mM EDTA) at a 1:1 molar ratio to reach final molarity 10μM. In addition, combinations of only 2 or 3 starting oligonucleotides were annealed to be used as molecular weight markers. The samples were annealed in a thermocycler (Eppendorf) under the following program:

Lid: 105°C WAIT AUTO
1. T=95°C 3min
2. T=65°C 2min
3. T=60°C 5min
4. T=60°C
   -1°C/0.5min x 40 repeat
5. HOLD @ 4°C ENTER
End

The annealed products was analyzed with 3% (w/v) agarose gel and stained with Ethidium Bromide (Pierce) DNA stain. Destaining was carried out by submerging the gel in fresh 1xTAE buffer and shake briefly for 10 min at 0.4 rmp. Analysis of the gel band was done with Kodak 1D software (Kodak). The efficiency of solution phase X-DNA formation was calculated by comparing the net intensity of X-DNA band with the total intensities from all bands on the gel lane. The sequences were also inputted into m-Fold for checking of sequence design accuracy and ΔG of formation.

Biotinylated spacer DNA was similarly annealed and subsequently immobilized onto avidin-coated 6% cross-linked agarose beads (Pierce) in PBS buffer and 0.1%SDS. To optimize immobilization, the spacer DNA concentration was titrated from 56 - 170M DNA / 50µl agarose bead, and the amount (in percentage) of DNA immobilized over 1, 2, 3 and 15 hrs at room temperature (~18°C) and 30°C were calculated from OD_{260} of supernatant and recorded. For this study, the mass of DNA / amount of agarose beads were kept fixed while the reaction volume (and therefore concentration of spacer DNA) and reaction temperature is varied.

Solution phase X-DNA was ligated onto spacer at 3:2 molar ratio overnight with T4 ligase (Promega) at 5x excess enzyme unit / mol DNA. The reaction was conducted at room temperature with frequent rotation to keep beads in suspension. The beads with ligated spacer and X-DNA were

centrifuged at 2,000 rcf for 2 min and supernatant removed. 5x volume of 1xPBS was added and mixed by repeated pipeting. Centrifugation and removal of supernatant was repeated 10x, and a final wash with ddH_2O completed the washing stage. Then, DdeI (Promega) digestion at 37^oC for 3hrs was performed to release the solid phase synthesized X-DNA from the spacer. The sample was centrifuged to suspend the beads. Solid phase X-DNA remaining in the supernatant was removed and purified from restriction enzyme reaction buffers by QIAquick PCR Purification Kit (Qiagen).

2.2.3 Characterization of X-DNA

The solid phase X-DNA was characterized by ligating to hpA' at 1:4 molar ratio using T4 ligase overnight at room temperature on benchtop. DNA was purifed using QIAquick PCR Purification Kit (Qiagen) and Exonucleus III (Promega) digestion was carried out with 40x excess enzyme unit / mol DNA for 15 min and 30min at 37^oC. ExoIII was deactivated by adding 2ul of 0.5M EDTA / 100 unit enzyme. Solution phase X-DNA was similarly ligated to hpA' and hpB' at 1:3:1 molar ratio and digested with ExoIII. This is to confirm the assembly of solution phase X-DNA and to use as molecular weight marker. The samples were run on a 3% (w/v) agarose gel and analyzed same as described above (solution phase X-DNA characterization). ExoIII activity was confirmed by digestion of pVax plasmid DNA. Digestion was carried out for 15 min at 37^oC and deactivated with EDTA (data not shown).

2.3 Results

2.3.1 X-DNA Solution Phase

Gel image of single starting olignucleotide (xo1), combination of 2 starting oligonucleotides x01/x02, 4 combinations of 3 starting oligonucleotides, and solution phase X-DNA is shown on Figure 2.4. Upward

mobility shift on the gel on lane 2 compared to lane 1 indicate that a larger molecular weight molecule formed, as expected. Other combinations of only 2 oligonucleotides were also made and analyzed on 3% agarose gel, all showing similar mobility shift (data not shown). Interestingly, for samples with combinations of 3 starting oligonucleotides, only samples with either x01 or x04 (but not both) result in a higher molecular weight species than combination of 2 starting oligonucleotides. This may be due to the shorter length of the x01/x04 arm (only 12bp) which is not sufficient to stabilize the structure. The addition of a fourth oligonucleotide (Lane 7, 8) forms a structure with a larger molecular weight than combinations of 3 starting oligonucleotides that was later proven to be X-DNA by hairpin and ExoIII characterization. Lane 8 holds 2x DNA (overloaded) as the previous to reveal any other minor products in the solution. An output using m-Fold shows this structure has a ΔG of -59.1kcal/mol after hybridization (Figure 2.5). No other alternative outputs were listed by the program.

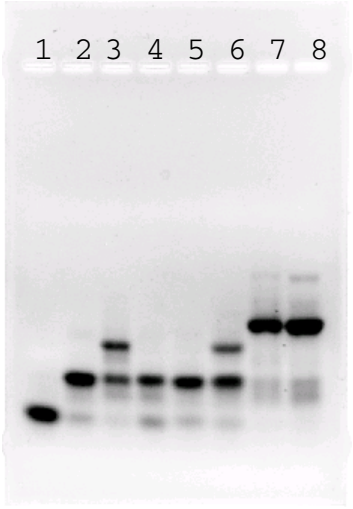

Figure 2.4 Solution Phase X-DNA Formation

Lane 1: x01, lane 2: x12, lane 3-6: x02/03/04, x01/03/04, x01/02/04, and x01/02/03, respectively, lane 7 and 8: solution phase X-DNA.

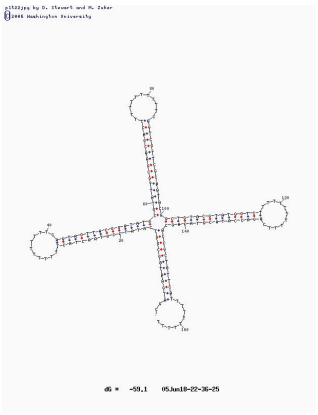

Figure 2.5 m-Fold Output of X-DNA Structure with Hairpins

Detection of bands in Kodak 1D at sensitivity=1, profile width = 65% showed there were only 3 types of product present, a larger molecule than X-DNA (band#1), solution phase X-DNA (band#2), and partially annealed (band#3) (Table 2.3). The percent in intensity of X-DNA band from lane 7 compared to total intensities indicated that X-DNA is the major product, with ~67.5% purity, while bands #1 and #3 contain 4.4% and 28.1% of sample mass. An intensity profile of lane 7 can be seen on Figure 2.4. The software detected 3 bands, which was fitted to a Gaussian model for calculation of mass (Figure 2.6). Note that these results were obtained with Ethidium Bromide stain, which is an intercalating dye that preferentially stains double stranded DNA.

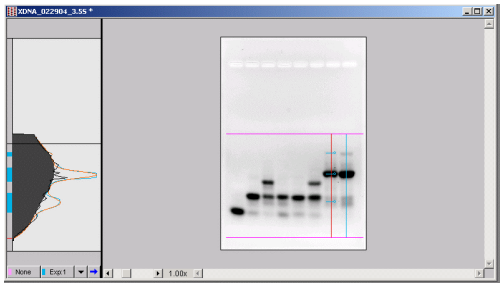

Figure 2.6 Gel Analysis on Kodak 1D v3.5 of Solution Phase X-DNA

Table 2.2 Yield Calculation for Solution Phase X-DNA

	Lane 7		Lane 8	
Band #	Band Intensities	Yield	Band Intensities	Yield
1	5.4274	4.40%	30.05	16.70%
2	83.75	**67.50%**	99.56	**55.50%**
3	34.92	28.10%	49.82	27.80%
Sum Intensity	124.0974		179.43	

Traces of partially formed structures on lanes 7 and 8, similar to combinations of 2 oligonucleotides, as well as larger complexes were also visible on the gel image. To simulate real conditions where numerous copies of oligonucleotides are present at once, multiple copies of oligonucleotides were inserted into m-Fold DNA folding program. Since only one input sequence is processed at a time, the sequences (x01-04) were entered; each separated by 10 T's to eliminate artificial constraints on the vertexes.

The folding program shows that, while X-DNA is the major product with lowest free energy after formation, another possible structure was presented that may explain the smear immediately above X-DNA band and clear band above it. (Figure 2.7). While Figure 2.7a shows the more stable structure as separate X-DNA's, Figure 2.7b depicts an alternative structure only 0.2kcal/mol higher in ΔG. This molecule results from arrangement of 8 oligonucleotides (2 sets of x01-04) into a starburst structure with 8 arms. The smear above X-DNA band may be incomplete formation of this structure. Larger structures were not produced by m-Fold when 3 or more sets of sequences were inputted, and were also not found on the gel. I speculate that the strain on the junction when more than 8 oligonucleotides are present would be too much to maintain a

stable structure. Also, while m-Fold is useful in listing out all possible arrangements of starting oligonucleotides, no programs to date accurately calculate contributions from structural factors such as steric hindrance of DNA junctions. This may explain the incongruity in ΔG and amount of product (67.5% X-DNA vs. 4.4% starburst DNA).

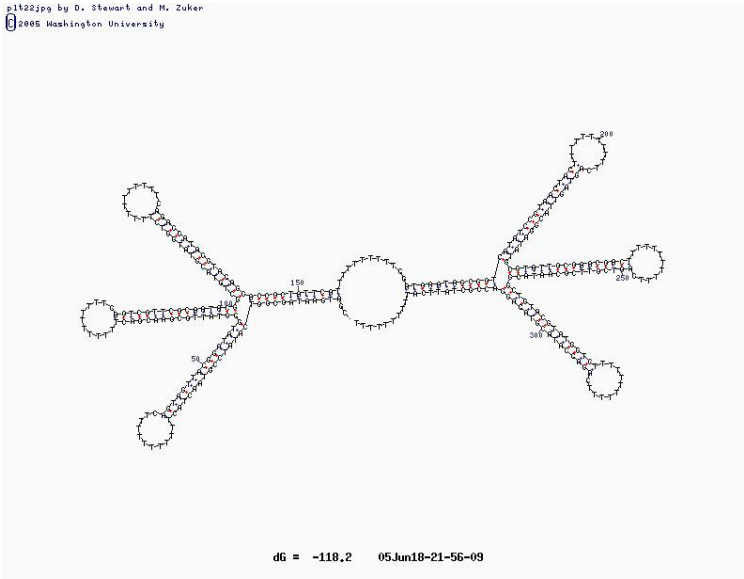

Figure 2.7a Major Product as Result of m-Fold Analysis of 2 X-DNA's (dG = -118.2kcal/mol)

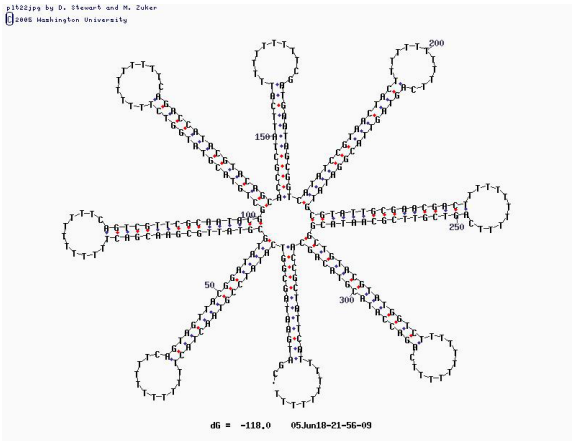

Figure 2.7b Starburst Structure from m-Fold analysis of 2 X-DNA's (dG=118.0)

2.3.2 Spacer Immobilization

The results for spacer DNA immobilization on streptavidin-coated agarose beads showed concentration based efficiency in attachment of biotinylated spacers to the beads. After 15hrs of mixing at room temperature (~18^{o}C), percent of spacer DNA attached to beads increased from 40% - 77%, directly in relationship to concentrations 2.0 – 6.0µg/µl (Figure 2.8). This is essentially a representation of biotin attachment to streptavidin as a function of concentration of biotinylated reactants. The trend in data points was found to be best fitted to an exponential one, with R^2 value of 0.959. This observation is interestingly in direct contrast to the well-known log-based relationship between substrate concentration and activity.

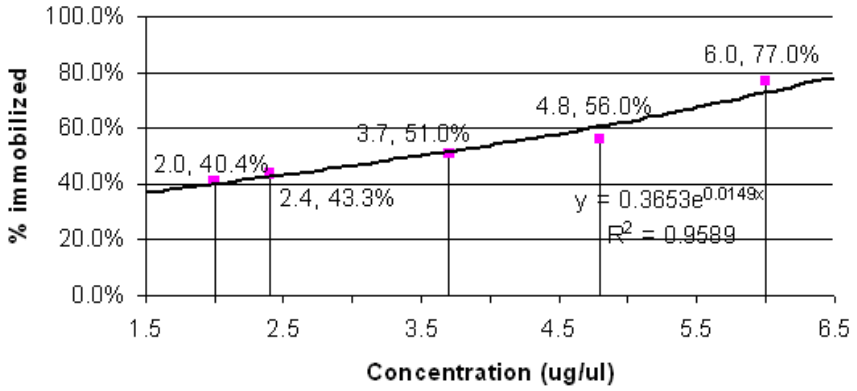

Figure 2.8 Concentration-Based Biotinylated DNA Attachment to Streptavidin-Coated Beads

Further studies on biotin-streptavidin attachment with respect to time and temperature revealed that neither plays a great role in the outcome. Figure 2.9 shows the percent of spacer DNA immobilized onto beads after 1, 2, 3, and 15 hrs for samples A, B, and C with concentrations 3.7, 4.8, and 6.0µg/µl, respectively (also see Table 2.2). It is evident that little difference can

be seen after 2 hrs of mixing, and the amount of DNA immobilized after 15 hrs for both sets of samples at room temperature and 30°C was comparably similar (at maximum 2% difference).

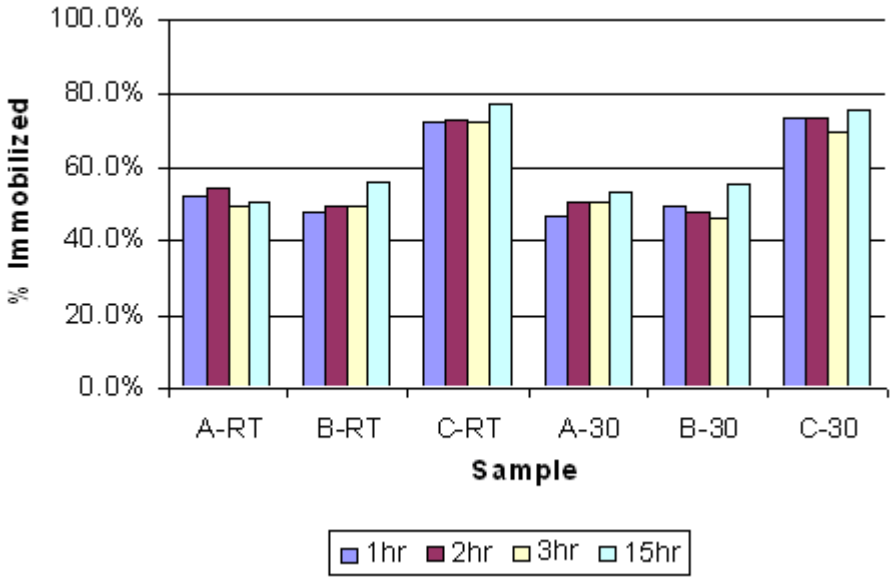

Figure 2.9 Time and Temperature Based Biotinylated DNA Attachment to Streptavidin-Coated Beads

Table 2.3 Time and Temperature Based DNA Attachment to Streptavidin-Coated Beads

	Sample	1hr	2hr	3hr	15hr	Concentration (ug/ul)
RT	A-RT	52%	54%	49%	51%	3.696
	B-RT	48%	50%	49%	56%	4.84
	C-RT	72%	73%	72%	77%	5.96
30°C	A-30	46%	51%	51%	53%	3.696
	B-30	50%	48%	46%	56%	4.84
	C-30	74%	74%	70%	76%	5.96

2.3.3 Solid Phase X-DNA Purity, Yield and Characterization

Lane analysis of Figure 2.10 revealed that solid phase X-DNA (lane 2) has only 2 bands (#1 and #2); the solid phase immobilization and washing steps successfully removed partially formed structures from the sample. The purity for solid phase X-DNA was 72.2%, higher than that of solution phase X-DNA (65.6%, lane 1, Table 2.3). The yield for solid phase X-DNA was ~14%. This low number is due to the many purification steps such as purification after enzyme reactions (T4 ligase and DdeI) and washing steps, which are necessary to produce pure X-DNA.

Table 2.4 Yield Calculation for Solution vs. Solid Phase X-DNA

	Solution phase X-DNA		Solid phase X-DNA	
Band #	Band Int.		Band Int.	
1	52.02	25.40%	49.96	27.80%
2	134.13	**65.60%**	130.04	**72.20%**
3	18.46	9.00%	--	--
Sum Int.	204.61		180	

Characterization of solution and solid phase X-DNA was conducted as previously described (see section 2.3). Lane 3 of Figure 2.10 shows ligated products of solution phase X-DNA to hpA'and hpB'. While most were ligated to form the closed circular structure, some partially ligated products were present. After 30 min of Exo III digestion of the sample, only 1 band was present on lane 4, while all other partially ligated (and thus not closed) structures were digested away. Similarly, lanes 5 and 6 for solid phase X-DNA characterization showed a single band after 15 and 30 min of digestion. The

intensities of these bands were close to similar (36 vs. 32), indicating that the mass of DNA species was unchanged over time, and that it is indeed the closed circular structure formed by ligation of X-DNA to hairpins.

The formation of solid phase X-DNA was confirmed by 2 points: 1) the gel analysis (Figure 2.4) that indicate the formation of this structure can only be formed by all 4 oligonucleoetides, and 2) the correct hybridization scheme produced arms with specific sticky ends that can be recognized by the inputted hairpins, which forms the circular structure that is impervious to Exo III digestion (Figure 2.10).

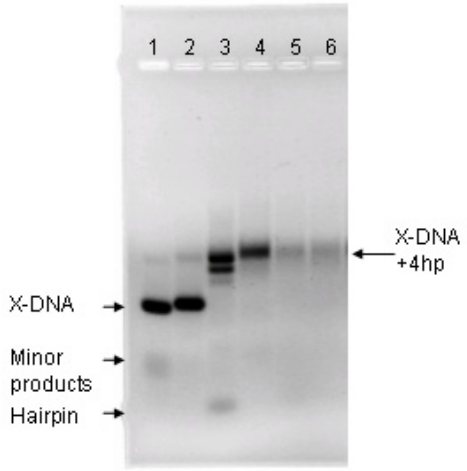

Figure 2.10 Characterization of Solution and Solid Phase X-DNA

Lane 1: Solution phase X-DNA, lane 2: solid phase X-DNA, lane 3: solution phase X-DNA ligated to 4 hairpins, lane 4: samples from lane 3 with 30 min ExoIII digestion, lane 5: Solid phase X-DNA with hpA' and ExoIII (15min), lane 6: Solid phase X-DNA with hpA' and ExoIII (30min)

2.4 Conclusion and Discussion

The study on solid phase synthesis of X-DNA revealed a new and method for making DNA building blocks. The advantages to this method lies in the built-in purification steps that is facilitated by bead immobilization and washing of non-specific binding (and not desired) products. Comparable

purities (65% for solution phase vs. 72% for solid phase) may be attributed to the sequence design, as well as annealing conditions, which could be further optimized. The low yield (~14%) must be addressed by introducing different means of purification from enzymatic reactions, since the column-based technique is not suitable for purifying small DNA molecules. The range for QIAquick PCR purification kit is 100bp-10kb, and X-DNA is 62bp—well below the minimum limit—and can not bind as tightly to the column.

Another difference between solution and solid phase synthesis is the cost. In solid phase synthesis, extra expenses such as spacer DNA, biotinylation, avidin-coated beads, enzymes, purification kits, and time must be considered. This leads to the conclusion that while this is not a suitable and cost-effective method for producing single building blocks, it is a powerful method for step-by-step building of larger structures like dendrimer-like DNA's. Solution phase ligation of DNA's result in several partial products (Figure 2.4), which can be readily eliminated when the structure is immobilized on a solid support. This is much more convenient, robust, and cheaper when compared to dendrimer-like DNA synthesis in solution, where each generation must be gel purified before further growth. Furthermore, this process can be fully automated, perhaps on a microfuildic device or chromatographic column setup with reusable spacer DNA. To minimize costs and improve yield and purity through experimental methods and sequence design would the next step in making solid phase synthesis a practical and accepted method for synthesis of complex structures with DNA as scaffold.

CHAPTER 3
PLASMID AMPLIFED DNA SYNTHESIS (PADS)

3.1 Introduction and Schematics

To meet the demand for high quality (purity and yield) DNA building blocks that are cheap and easy to produce, an alternative approach to solution and solid phase synthesis was taken. Plasmid amplified DNA synthesis, or PADS, utilizes the natural ability to reproduce plasmid DNA in bacteria as a mechanism for production of DNA building blocks.

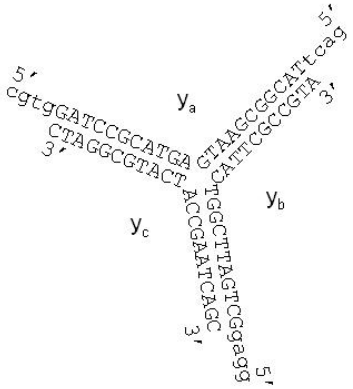

Figure 3.1 Y-DNA

More specifically, Y-DNA sequence is cloned into pZero plasmid (Invitrogen) by mini-circle cloning method. Y-DNA is a building block with 3 dsDNA branches, much like the DNA replication fork (Figure 3.1).
The first step involves circularizing the Y-DNA by ligation to 3 arms to hairpin loops. The resulting molecule, called hpY, is topographically closed (does not contain open sticky ends) and could be purified from solution by ExoIII digestion. A complementary version of Y-DNA (called CY-DNA) ligated to hairpin loops is similarly synthesized and annealed to the first to form a mini-circle. This circle can then be linearized and inserted into bacteria plasmid for transformation. The bacteria's multiplication and DNA replicating mechanisms

amplify the amount of plasmid, such that a large number of plasmid encoding Y-DNA could be harvested after incubation in growth media (Figure 3.3a).

Y-DNA is formed and released by first nicking one strand of the plasmid. This is accomplished by a modified restriction enzyme that recognizes a unique 7bp sequence and cuts only one strand on a dsDNA upon binding. The nicked DNA strand is then digested away using Exonuclease III (or ExoIII) that cleaves covalent phosphodiester bonds that link nucleotides from the 3' end of the DNA molecule. Only one strand is left of the plasmid, which is then annealed at low concentration to form Y-DNA with hairpin loop structure (Figure 3.3b). Y-DNA is subsequently released by restriction enzyme digestion, which recognition sites are pre-programmed into each arm of the molecule. (Figure 3.2) The harvested Y-DNA's can then be used for a number of applications, such as scaffolding, or anisotropic attachment of molecular components due to the uniqueness of each sticky end.

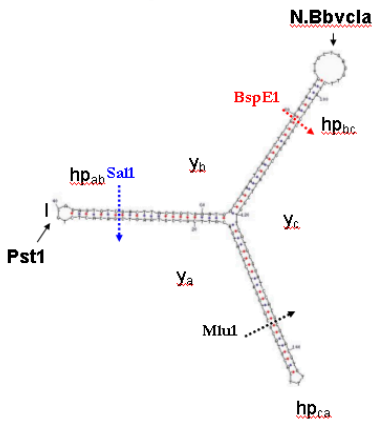

Figure 3.2 Restriction Enzyme Sites on Hairpin Loop

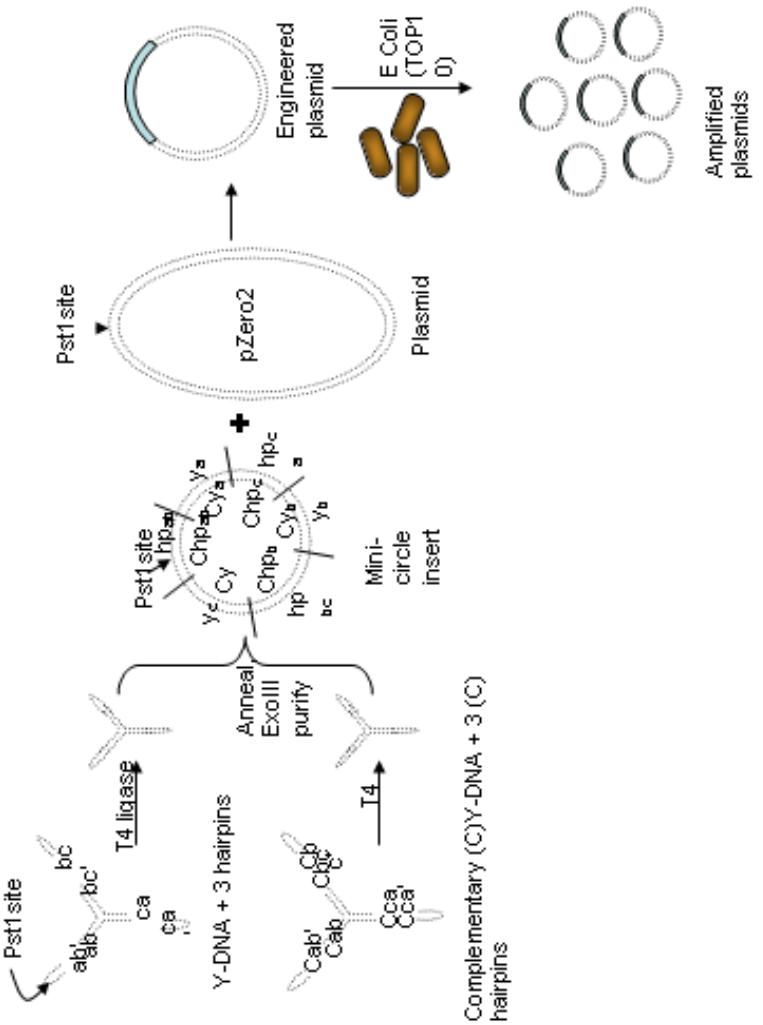

Figure 3.3a Schematic for Y-DNA Cloning into E Coli

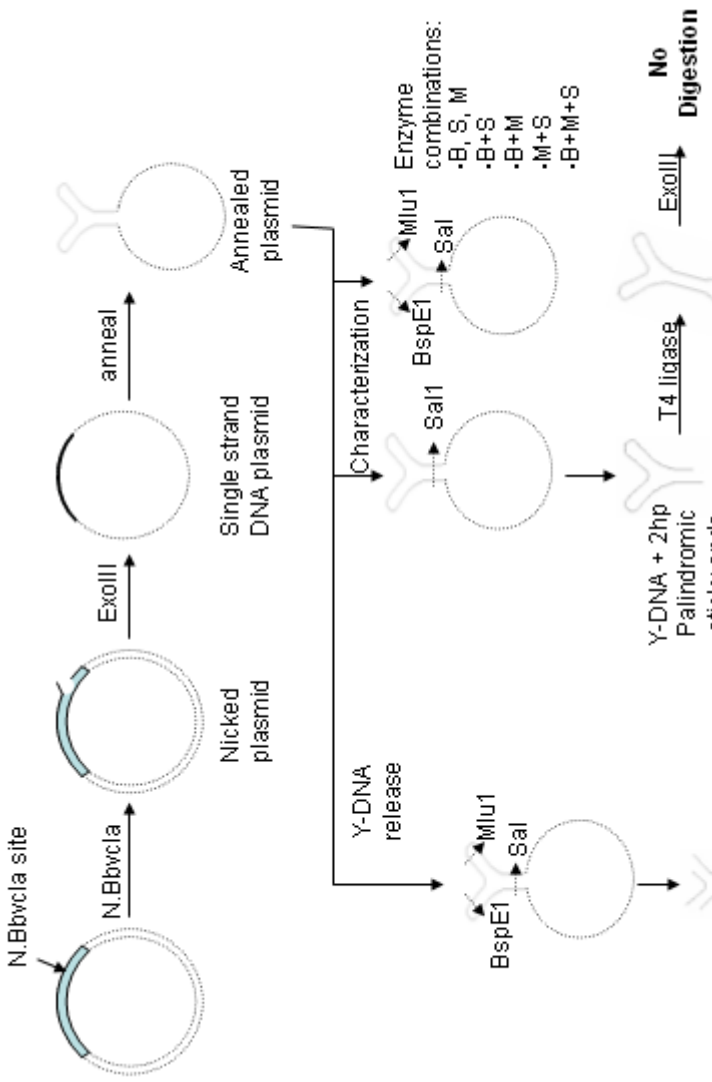

Figure 3.3b Schematic for Y-DNA Harvest and Characterization

Table 3.1Y-DNA and Hairpin Sequence

Structure	Name	Sequence (5'→3')	Length (nt)	MW (g/mol)
Y-DNA	y_a	CGT GGA TCC GCA TGA CAT TCG CCG TA	26	8027.2
	y_b	GAC TTA CGG CGA ATG ACC GAA TCA GC	26	8069.2
	y_c	GGA GGC TGA TTC GGT TCA TGC GGA TC	26	8138.2
hairpins	hp_{ab}	AGT CGA CAC TCT GCA GAG TGT C	22	6815.4
	hp_{bc}	CTC CGG ACA TAG TTG CTG AGG TTC TAT GTC C	31	9573.2
	hp_{ca}	CAC GCG TAC GTG TTT CAC GTA CG	23	7095.6
Complementary Y-DNA	Cy_a	TAC GGC GAA TGT CAT GCG GAT CCA CG	26	8076.2
	Cy_b	GCT GAT TCG GTC ATT CGC CGT AAG TC	26	8033.2
	Cy_c	GAT CCG CAT GAA CCG AAT CAG CCT CC	26	7965.1
Complementary hairpins	Chp_{ab}	GAC ACT CTG CAG AGT GTC GAC T	22	6815.4
	Chp_{bc}	GGA CAT AGA ACC TCA GCA ACT ATG TCC GGA G	31	
	Chp_{ca}	CGT ACG TGA AAC ACG TAC GCG TG	23	7153.6

The characterization method for PADS involves restriction enzyme mapping, where different combinations of restriction enzymes that digest the arms of the Y-DNA is applied. Ligation of Sal1 digested structures and digestion with ExoIII also add to this result (Figure 3.3b). The electrophoresis mobility shift on normal and denaturing agarose gel is used to confirm the formation of Y-DNA from the plasmid.

3.2 Experimental Methods

3.2.1 Design and Synthesis

Y-DNA was made from 3 oligonucleotides, y_a, y_b and y_c, that are partially complementary, such that their hybridization form a 3 armed dsDNA structure (Figure 3.1).(Li, Tseng et al. 2004) The sequence has been shown to be robust in forming Y-DNA in solution. The hairpins, hp_{ab}, hp_{bc} and hp_{ca}, were designed to form a 10bp stem with a 3 Thymine bases as loop. The sequences for complementary oligonucleotides were determined as indicated by its name—which are sequences directly complementary to Y-DNA and hairpins (Table 3.1).

The starting oligonucleotides were annealed as described in Chapter 2.3. Following electrophoresis to confirm the formation of Y-DNA and hairpins, they were ligated using T4 ligase (Promega) at 1:1 molar ratio (Y-DNA:hairpin) at room temperature overnight on bench top. The same procedure was repeated for the complementary (C) version of Y-DNA and hairpins.

ExoIII (Promega) digestion was carried out directly after ligation at 40x enzyme excess for 15 minutes at 37^{o}C and deactivated by addition of EDTA (2ul 0.5M EDTA / 100 unit of enzyme). Following digestion, the sample was purified from enzyme and buffer by QIAquick PCR Purification kit (Qiagen).

Annealing of hpY and ChpY at 1:1 molar ratio was done by the following program (YENANEL) in a thermocycler:

Lid: 105°C WAIT AUTO
6. T=95°C 3min
7. T=90°C 2min
8. T=90°C
   -1oC/min x40 repeat
9. T=50°C
   -1°C/min x 40 repeat
10. HOLD @ 4°C ENTER
END

The formation of hpY was confirmed by redigestion with respective restriction enzymes, and by ExoIII digestion to indicate disruption of the closed loop (hpY) by these enzymes.

3.2.2 Cloning and Harvesting of Plasmid

After annealing, the sample and pZero2 (Invitrogen) was linearized with the restriction enzyme Pst1 (New England Biolabs) for 2hrs at 37°C. The samples were purified using QIAquick PCR purification kit, and ligated at 1:1 molar ratio (30 femto moles plasmid : 30 femto moles insert) with 5x excess T4 Ligase at room temperature overnight. Note that the plasmid pZero2 is part of the Zero Background cloning kit, part of the Gateway cloning system (Invitrogen), which reduces false positives by the presence of the ccdB gene in uninserted plasmids. The ccdB protein is a natural analogue of quinolone antibiotics, which binds to DNA helicase subunit A to inhibit the activity of this protein (Critchlow 1997). Due to the high efficiency in screening, introduced by this property, no dephosphorylation was necessary.

Following ligation, 20ng of DNA was electroporated into TOP10 bacteria. The bacteria was incubated at 37°C for 1 hr in vigorous agitation (250rpm) in SOC medium and plated at 25ul and 50ul onto SOC +

Kanamycine agar plates. Pure pZero plasmid was also plated as a negative control. The plates were incubated upside-down at 37^{o}C for 15 hrs.

Colonies that appeared on the plates were picked up and inoculated separately in 3ml LB + Kanamycine broth at 37^{o}C, 250rpm, for 15 hrs. The plasmids were purified from bacteria using Eppendorf MiniPrep Kit (Eppendorf) and eluted in ddH2O. Confirmation of successful cloning of the Y-DNA mini-circles was achieved by digestion of harvested plasmid with Mlu1 (New England Biolabs) which is only present on the insert (Figure 3.2). The reaction was carried out in 50ul for 200ng DNA and 5x excess enzyme, at 37^{o}C for 1hr. The samples were run with an undigested and digested plasmidm and pZero plasmid incubated with Mlu1, on 1% (w/v) agarose gel in TAE buffer as negative and positive controls.

The number of insert was confirmed by digestion of 2 restriction enzymes that flank the cloning site, ApaI and HindIII. The mobility shift for the digested DNA fragment was run and compared to a 100bp ladder on a 3% (w/v) agarose gel, in TAE buffer.

3.2.3 Y-DNA Production and Characterization

A larger batch of a single positive colony was made for Y-DNA harvest and characterization. Colony 25A was inoculated in 50ml LB + Kanamycine (LBK) media and incubated at 37^{o}C, 250rpm agitation overnight. Following initial incubation, the entire volume was added to 600ml of LBK and incubated for ~8hrs until the concentration of bacteria is sufficiently grown (1.0-2.5 OD600). Bacteria plasmid was extracted and purifed using Eppendorf MaxiPrep Kit (Eppendorf).

25A plasmid was nicked with N.BbvcAI (New England Biolabs) at 37^{o}C for 3 hrs, at 5x excess enzyme, to ensure complete digestion. ExoIII was

added to the reaction and buffer content adjusted accordingly. The duration for exoluclease reaction was 15 min at 37^{o}C, followed by 20min incubation at 75oC to deactivate the enzyme. The sample was ethanol precipitated to concentrate DNA, which was resuspended in ddH2O. Result for enzyme activity (nicking and exonuclease) was evaluated by gel electrophoresis on 1% (w/v) agarose gel in TAE buffer at 100V and 60min, and DNA visualized using Ethidium Bromide stain.

The single stranded plasmids are then annealed using the program YENANEL (see 3.2.2) at low concentration (17-25nM) to prevent intermolecular hybridization. Production of Y-DNA was done by simultaneous digestion by all 3 enzymes, Sal1, Mlu1, and BspE1 (New England Biolabs), to release Y-DNA. The samples were concentrated by ethanol precipitation and resuspended in ddH2O. Characterization of the product was achieved by a digestion using different combinations of the above 3 enzymes. The samples were first annealed at low concentration, and freeze-dried to reduce the sample volume. Single restriction enzyme digestion by 3 enzymes, Sal1, Mlu1, and BspE1 were conducted, as well as combinations of restriction enzymes: Sal1+Mlu1, Sal1+BspE1, Mlu1+BspE1 and all 3 enzymes. The digested oligos were run with enzyme and buffer on 3% (w/v) agarose gel in TAE buffer at 85V, for 120min and 2 hrs of staining with SYB1R1.

Sal1 digested annealed ssDNA plasmids were gel purified (Qiagen) and ligated overnight at room temperature. ExoIII digestion of ligated oligos were carried out at 37^{o}C for 15min, followed by deactivation at 75^{o}C for 20min. The samples were run on a 4% (w/v) agarose gel with TAE buffer at 90V for 120min in 4^{o}C. Similar experiment was done without gel purification and similarly ligated, ExoIII digested, and visualized in agarose gel.

3.3 Results

Gel electrophoresis confirmed the formation of Y-DNA on a 3% (w/v) agarose gel. Figure 3.4 shows hairpin before and after annealing (Lanes 2 and 3) and the step by step combination of oligonucleotides (Lane 4: y_a serves as molecular weight marker), into partial structures (Lane 5 and 6: y_a+y_b, y_b+y_c) and finally Y-DNA (Lanes 7 and 8). The single clear band on Y-DNA lane indicates that a pure species of higher molecular weight formed from these 3 oligonucleotides.

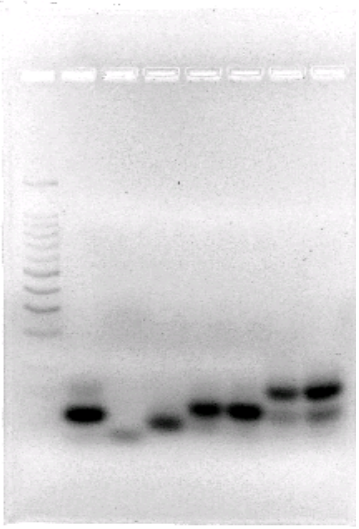

Figure 3.4 Solution Phase Y-DNA
Lane 1: 100bp ladder, lane 2: unannealed hairpin, lane 3: annealed hairpin, lane 4: y_a, lane 5 and 6: ya/b, yb/c, and lanes 7-8: Y-DNA once and twice loaded in mass.

The characterization of Y-DNA by hairpin ligation and digestion (Figure 3.5a) and ExoIII digestion shown in Figure 3.5b confirms the correct formation of hpY with all 3 enzyme digestion sites. Figure 3.5a shows annealed hairpin and Y-DNA on lanes 1 and 2. Lane 3, used as molecular weight marker, shows Y-DNA with 2 hairpin loops. Lane 4 and 8 contain hpY, and lanes 5-7 shows digestion of hpY with Sal1, Mlu1, and BspE1 respectively. Figure 3.5b

shows oligos from lanes 4-8 of Figure 3.5a after ExoIII digestion. Successful digestion of all single enzyme digested samples indicate that the closed loop has been broken, but the flanking lanes 2 and 6, which contain hpY, was not digested. Lanes 1 and 7 contain hpY as marker.

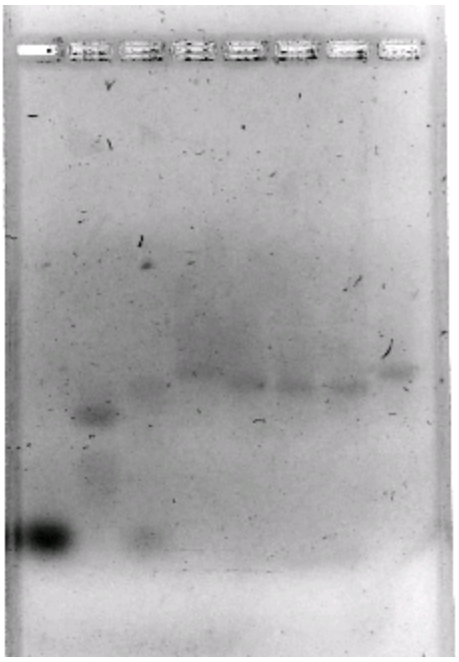

Figure 3.5a Annealed and Digested hpY

Lane 1: Annealed hairpin DNA, lane 2: Y-DNA, lane 3: Y-DNA and 2 hairpins, lane 4 and 8: hpY, and lanes 5-7: hpY digested with BspE1, Mlu1, and Sal1.

Figure 3.5b ExoIII Characterization of hpY

Lanes 1 and 7, lanes 2 and 6: hpY + ExoIII, lanes 3-6: Lanes 5-7 of Figure 3.5a after ExoIII digestion

The making of insert (Figure 3.6a) shows some higher molecular weight species occurring after hybridization (Lane 6). This is evident after band detection by the Kodak 1D software (band sensitivity = 0 (normal), profile width = 79%) as shown in Figure 3.6b. However, the major product remains hpY species. Cloning of the insert (Lane 7) with linearized plasmid (Figure 3.6c, lane 3) produces a total of 4 colonies, all of which contain the engineered plasmid 25A, 25B, 50A, and 50B (100% cloning efficiency) and screened by Mlu1 digestions (Figure 3.7). Experiment to determine the number of insert indicates that only one insert is present in the engineered plasmid. Since the distance between Apa1 to HindIII is 104bp, and the insert length is 142bp, the total distance for digested fragment containing a single insert is 246bp, which is roughly the size of fragment present on Figure 3.8, lane 3.

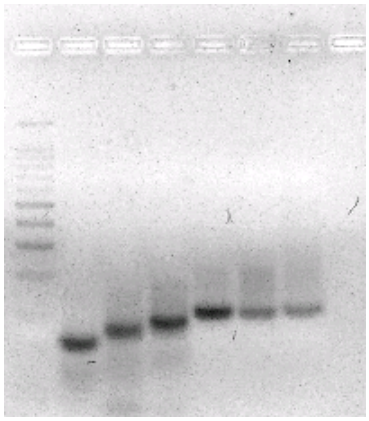

Figure 3.6a Y-DNA Insert

Lane 1: 100bp ladder, lane 2: Y-DNA, lane 3 and 4: Y-DNA with 1 (hpab) and 2 (hpab + bc) hairpins, lane 5: hpY, lane 6: hpY + ChpY, and lane 7: hpY + ChpY after Pst1 digestion.

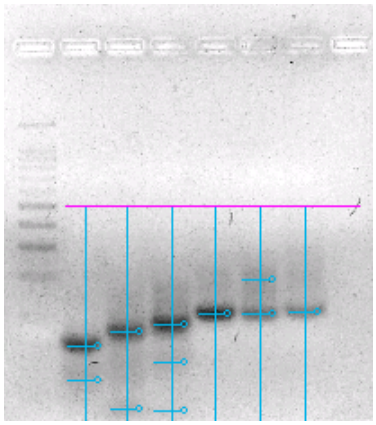

Figure 3.6b. Y-DNA Insert Band Analysis

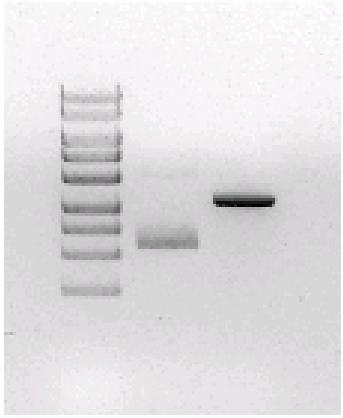

Figure 3.6 c pZero-2 Plasmid

Lane 1: 1kb ladder, lane 2: supercoiled pZero-2, and lane 3: pZero-2+Pst1

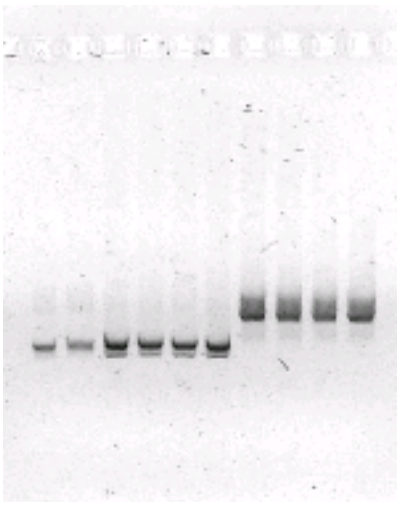

Figure 3.7 Screening of Electroporated Top10 Colonies

Lane 1: pZero-2, lane 2: pZero-2+Pst1, Lanes 3-6: Plasmids 25A, 25B, 50A, 50B, and lanes 7-10: plasmids from lanes 3-6 after Pst1 digestion.

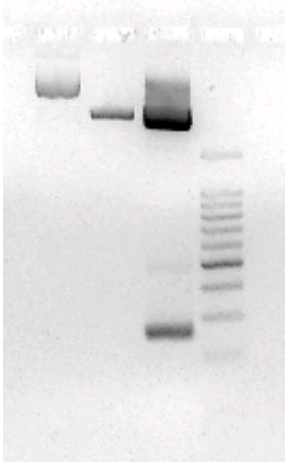

Figure 3.8 Insert Number on 25A Plasmid

Lane 1: pZero-2, lane 2: pZero-2+Apa1, lane 3: pZero-2+Apa1+HindIII, and lane 4: 100bp ladder.

Cultivation and purification of plasmid 25A produced ~1mg plasmid DNA from 650ml LB+Kanamycine medium. Nicking and synthesis of single-stranded DNA plasmid was shown in Figure 3.9. The reduced molecular weight to roughly ½ that of original size but not disappearance after digestion, indicated that a closed loop single stranded DNA molecule has formed. The resulting ssDNA size is ~1.7kb, about half of the original pZero plasmid (3.3kb).

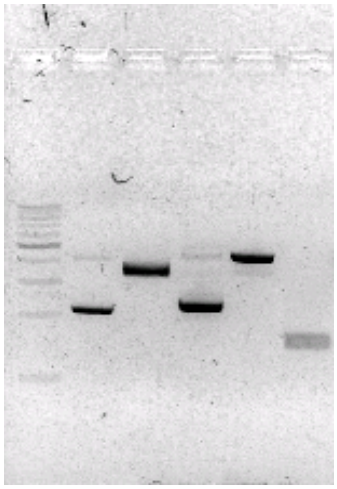

Figure 3.9 ssDNA Plasmid Synthesis

Lane 1: 1kb ladder, lane 2: pZero-2, lane 3: pZero-2+Pst1 (linear), lane 4: 25A plasmid, lane 5: 25A plasmid + N.BbvcA1, and lane 6: lane 5+ExoIII

Annealed ssDNA was digested with 3 enzymes (Figure 3.10, lanes 4-7) and only Sal1 (Figure 3.11a, lanes 2-8, Figure 3.11b, lanes 4-5). The DNA produced after digestion for Figure 3.10 showed 2 clear bands, one corresponding to Y-DNA, and one smaller, that correspond to a partial Y-DNA structure (2 oligonucleotides) that is shown faintly below the Y-DNA band on lane 2. The annealed plasmid without digestion is shown on lane 3, and no oligos of similar molecular weight to Y-DNA was present in the sample prior to

enzyme digestion. This may be due to the harsh purification environment with ethanol precipitation, where excessive drying of sample lead to denaturation of DNA. Sal1 digestion (Figure 3.11a, b), on the other hand, shows a band corresponding to Y-DNA and 2 hairpins (Figure 3.11b, lane 3), and another band above it. Though dimerization (self-hybridization due to palindromic sticky ends) is possible, this should also be seen in the previous figure (Y-DNA production using 3 enzymes) and to a greater extent since there are 3 palindromic ends. It must also be noted, that the samples were prepared in different batches, which has conditions that may be favorable for dimerization but not the other.

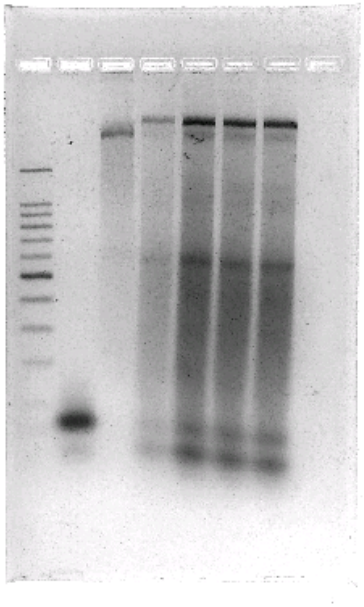

Figure 3.10 Y-DNA Production by Digestion with 3 Enzymes

Lane 1: 100bp ladder, lane 2: Y-DNA, lane 3: ssDNA plasmid, and lane 4-7: ssDNA plasmid + BspE1, Mlu1, and Sal1.

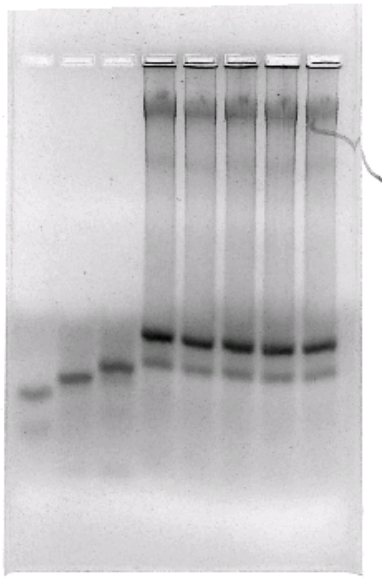

Figure 3.11a ssDNA Plasmid with Sal1

Lane 1: Y-DNA, lane 2-3: Y-DNA with 1 and 2 hairpins, and lanes 4-8: ssDNA + Sal1

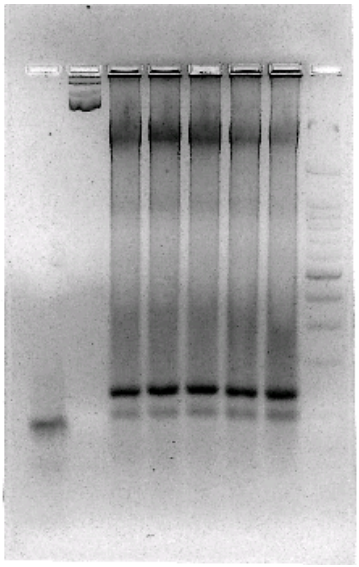

Figure 3.11 b ssDNA Plasmid with Sal1

Lane 1: Y=DNA with 2 haripins, lane 2: ssDNA plasmid, lanes 3-7: ssDNA + Sal1, and lane 8: 100bp ladder

Figure 3.12 shows the gel extracted L (lower) band and U (upper) band after T4 ligation and ExoIII digestion. Lane 4 and 6 looks remarkably similar, which may indicate the ligation process produced dimers of L bands (Lane 3), but no dimers could be produced for U bands (lane 6) since there are no available sticky ends after dimerization. (Figure 3.3b) However, the percentage gel is too low to clearly resolve this band. Figure 3.13a shows digested ssDNA plasmid with Sal1 (Lane 4, 7). After ligation (Lanes 5, 8), the oligos were digested by ExoIII to reveal a single band as detected by the Kodak 1D software (Lanes 6, 9) (sensitivity = 1, profile width = 79%) on Figure 3.13b. Lanes 7-9 are simply lanes 4-6 twice loaded. The remaining band after ExoIII digestion is about 200bp, indicated by the 100bp ladder (Lane 1), which is 2 times the size of the cut out structure, consistent with the size of the expected product, the dimerization of Y-DNA with 2 hairpins.

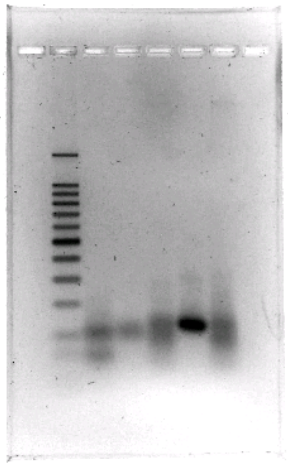

Figure 3.12 ssDNA Plasmid Sal1 Characterization

Lane 1: 100bp ladder, lane 2: Y-DNA with 2 hairpins, lane 3: lower band (lane 4, Figure 3.11a), lane 4: lane 3 + T4 ligase + ExoIII,, lane 5: upper band (lane 4, Figure 3.11a), and lane 6: lane 5 + T4 ligase + ExoIII.

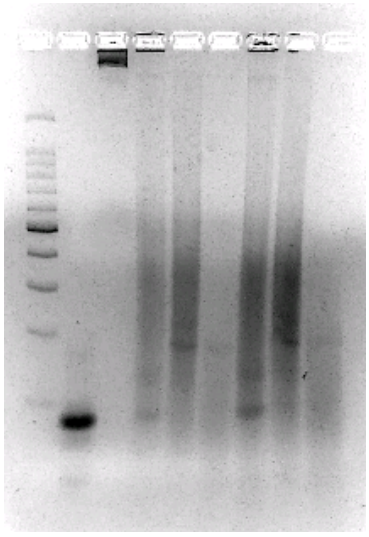

Figure 3.13a ssDNA Plasmid Sal1 Characterization with 4% gel

Lane 1: 100bp ladder, lane 2: Y-DNA with 2 hairpins, lane 3: ssDNA plasmid, lane 4: lane 3 + Sal1, lane 5: lane 4 + T4 ligase, lane 6: lane 5 + ExoIII, and lanes 7-9: lanes 4-6 twice loaded in mass

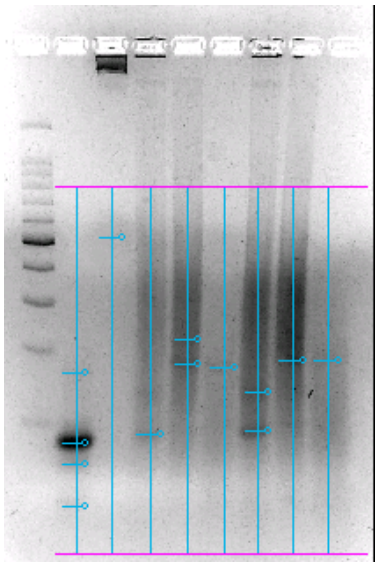

Figure 3.13b Band Analysis of Figure 3.13a

The annealed ssDNA was also digested with a combination of enzymes as shown in Figure 3.14a. Lanes 1 to 4 shows the hairpin structure, Y-DNA and additions of 1 and 2 hairpins. Lane 5 is the undigested ssDNA plasmid, and Lanes 6-8 shows ssDNA plasmid digestion with BspE1, Mlu1, and Sal1. All of the digested ssDNa plasmid shows bands below 100bp, but the staining did not resolve clear bands, since the percentage gel required long running and staining time, during which diffusion of the DNA from the band takes place. Single digestion with BspE1 and Mlu1 produced structures larger than hairpin, and a band similar size to hairpin was also seen on Mlu1. Since the hairpin loops are palindromic, the larger size maybe hairpin dimers. Digestion with Sal1 did not produce any clear bands for analysis.

Figure 3.14b is combination of restriction enzyme digestions on ssDNA plasmid. Lane 2 is the annealed hairpin, lanes 3 and 4 are Y-DNA and Y-DNA with 2 hairpins, lanes 5, 6 and 7 are combinations of 2 enzymes: BspE1+Sal1, Mlu1+BspE1, and Mlu1+Sal1, and lane 8 is digestion with all 3 enzymes. Digestion with BspE1+Sal1 produce molecules with similar molecular weight to Y-DNA, and a molecule 2 times larger than hairpins (similar size to partial Y-DNA). Digestion with Mlu1+BspE1 show only the latter band. Since the only possible digestion out of the ssDNA plasmid are hairpins, according to the schematic, the presence of this band could indicate actual hairpin dimers. Digestion with Mlu1+Sal1 produce 2 bands, 1 similar to Y-DNA, and the other similar to that on Lane 6, digestion by BspE1+Mlu1. Finally, digestion with all 3 enzymes show a single band similar size to the partial Y-DNA structures seen on Lane 3. The result of this gel is rather vague. Denaturation and dimerization may have occurred as result of ethanol precipitations and resuspension process (sample temperature raised to 37^{o}C and reduced to 4^{o}C).

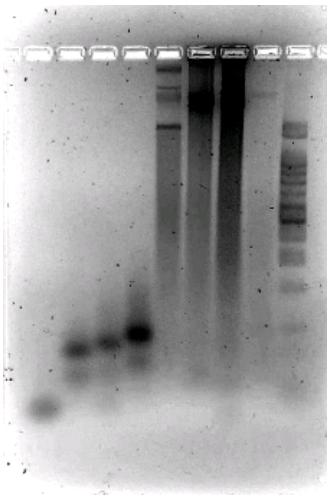

Figure 3.14a ssDNA Plasmid 3 Enzyme Characterization

Lane 1: hairpin DNA, lanes 2-4: Y-DNA, Y-DNA with 1 and 2 hairpins, lane 5: ssDNA plasmid (undigested), lanes 6-8: ssDNA plasmid + BspE1, Mlu1, and Sal1, and lane 9: 100bp ladder.

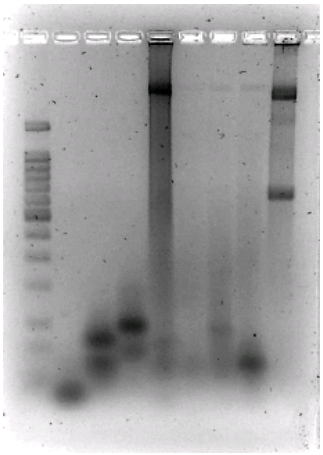

Figure 3.14b ssDNA Plasmid 3 Enzyme Characterization

Lane 1: 100 bp ladder, lane 2: hairpin, lane 3: Y-DNA, lane 4: Y-DNA with 2 hairpins, lanes 5-7: ssDNA plasmid +BspE1+Sal1, Mlu1+BspE1, and Mlu1+Sal1, lane 8: ssDNA plasmid + all 3 enzymes, and lane 9: ssDNA plasmid + Sty1 (unrelated).

3.4 Conclusion and Discussion

One of the main motivations behind PADS was to design a process for making a large amount of building-block Y-DNA cheaply. A brief cost comparison for between solution phase DL-DNA synthesis reveals that there are significant differences between the two methods. Solution phase DL-DNA synthesis involves annealing and ligating of Y-DNA. The oligos ordered has an expected yield of 4g/mol, for a range of molar concentrations (Chapter 1). For oligonucleotides below 40bp, the expected purity is over 95%, as specified by manufacturer. Thus the main factor affecting cost is annealing efficiency (set at 67.5%, Chapter 2) and ligation efficiency—which is assumed to be 100%.

In contrast, the PADS method relies on bacterial replication of building block DNA, thus the major cost is from bacteria media and enzymes to produce the DL-DNA from plasmid DNA. There are one-time costs, which is the expenses for preparation of stock colony with the engineered plasmid, including cloning kit (plasmid, E Coli, and enzymes), starting oligonucleotides and agar plates. Preparation costs include nicking enzyme and hairpin cleaving enzymes. One cost that is omitted from both methods is purification. This cost varies with design of the DNA building block. Non-palindromic building blocks qualifies for methods such as solid phase purification, which is cost saving due to reusable spacers, whereas DNA's with palindromic sticky ends must be purified by gel extraction.

Tables 3.2 and 3.3 summarizes these costs. For 1mg of G1 (Y-DNA), solution phase synthesis and PADS are comparable, at $393 to $401 respectively. However, as the generation number increase, the cost difference grows significantly larger. Each phosphorylated oligonucleotide of 30bp cost $25.8, and hairpins used for PADS are $24.6, as quoted by IDTDNA. These

numbers are used for calculating the cost of starting material in Tables 3.2 and 3.3.

Table 3.2. Solution Phase Cost Summary

	G1	G2	G3
Oligos	3	12	30
	77.4	309.6	774
Expected yield (ug)	291.6	1140	2850
$/mg DNA	265	272	272
After annealing (67.5%)	393	1308	30356
T4 ligase	NA	150	450
Number of sticky ends		3	9
Total cost ($)	393	1458	30806

Annealing efficiencies for 4 Y-DNA's (G2) and 10 Y-DNA's (G3) is compounded and affects the cost exponentially. The amount of enzyme (T4 ligase, Promega), also increase with the generations of Y-DNA. Purification costs are also not included; however in previous publication (citation), purifications by gel extraction were used between each addition of Y-DNA layer. The cost for 1mg pure G2 is $272/0.67.5^4 = $1308, and pure G3 is $272/0.67.5^10 = $30,356.

PADS costs are dramatically smaller, as the major cost is in starting oligonucleotides. Since only 1 copy of the correct insert is needed, efficiency is not a large factor in this step, and the cost—listed under "one time cost" is not considered in long term preparations. Also, as the mass ratio of insert DNA increase with respect to the plasmid DNA, more DNA is produced for the same amount of double stranded plasmid DNA. Though this translates to more enzymes needed for releasing DL-DNA from the plasmid, less media and

Table 3.3. PADS Cost Summary

		G1	G2	G3
One time	LB agar	0.11879	0.11879	0.11879
	pst1	0.058	0.058	0.058
	Kanamycin	omitable	omitable	omitable
	Cloning kit	330	330	330
	T4 ligase	10	10	10
	Exo III	omitable	omitable	omitable
Oligos	y oligo (25.8)	3	12	30
	hp (24.6)	3	6	12
		151.2	457.2	1069.2
	Oligo cost	302.4	914.4	2138.4
	Total oligos	6	18	42
Preparation	LB broth	228.691125	76.23038	32.67016
	Sal1	21.2	42.4	84.8
	Mlu1	46.4	92.8	185.6
	BspE1	46.4	92.8	185.6
	N.BbvcAI	58	116	232
	ETOH	omitable	omitable	omitable
	Exo III	omitable	omitable	omitable
	Eppendorf Maxi Prep	10.8	10.8	10.8
Cost ($/mg core Y-DNA)		714	1346	2870
Prep $ only		411	431	731
$/mg DL-DNA		714	336	287
Preparation $/ mg DNA		411	108	73

bacteria preparation (plasmid purification and ssDNA production) is needed. The total cost (including one time costs) for G1 bacteria is $714, but only $411 in expense is required for preparations of G1 (Y-DNA) once stock bacteria is made. G2 total cost is $336, and only $108 excluding bacteria preparations. The cost for G3 is $287 and $73 respectively. This cost, similar to solution phase synthesis, does not include purification from enzyme or leftover hairpin and ssDNA plasmid in the solution. The assumption is that these costs would be similar to both cases and will not affect the difference in the costs of the two methods. Also, the efficiency of purification is also a factor in cost calculation.

For the design proposed in this chapter, the sticky ends are palindromic. This brought some problems during characterization and purification process. The possibility of dimerization of products (Y-DNA or hairpins) makes it difficult to purify by solid phase. The gel extraction procedure (Qiagen) involves raising the temperature of the solution to higher than 50^{o}C, which destabilizes the small Y-DNA's. In addition, the size of Y-DNA is too small to efficiently bind to the purification columns, thus much DNA is lost in this process.

One major setback for PADS compared to solution phase synthesis of lower generation DL-DNA is time of preparation. Excluding plasmid preparation and cloning, the inoculation, growth, and purification of plasmid takes 3 days. Following ssDNA synthesis (1 day and 1 additional day for ethanol precipitation), the annealing and digestion takes 1-3 days, depending on the purification process (1 day for gel extraction, and 2 days for ethanol precipitation. The total time for preparation of one batch of DNA is roughly 1 week. In contrast, the total time for annealing Y-DNA is 30min for solution phase synthesis. With each generation growth, 1 day is taken for ligation

(overnight at room temperature). As DL-DNA generation grows, the time for preparation of solution phase eventually catches up to, and surpasses that of PADS.

Future design with non-palindromic ends may hold the solution to this problem. Unique sticky ends also enable the application of solid phase purification, similar to that described in Chapter 2. The immobilized spacers could be packed in a column format that is reusable to help reduce cost and increase production volume. The experiment in this chapter has shown that it is possible to clone and produce DNA building blocks from bacteria amplified plasmids.

CHAPTER 4
DNA FLUORESCENT NANOBARCODE

4.1 Introduction

The anisotropic, controlled self-assembly of DNA makes it an ideal nanoscale scaffolding material. A nanoscale fluorescence-based biosensor using dendrimer-like DNA (DL-DNA) scaffolding was successfully developed (Li, Cu et al. 2005), and shown to have multiplexed and rapid detection of molecules at attomole level. A separate study has also shown the capability of the nanobarcode as single molecular detector.(Stavis et al) In this chapter, I will describe a detailed study of the DNA fluorescent nanobarcodes, with respect to their purity, codability, and properties under harsh environment conditions. This characterization is important to evaluate the possibility of using DNA nanobarcode in actual biosensing applications in vitro, in vivo or for environmental monitoring purposes.

4.2 Bead Hybridization Scheme

The DNA fluorescent nanobarcode consists of 2 different color fluorophores Alexa Fluor 488 (Ex = 495 nm and Em = 519 nm) and BODIPY 630/650 (Ex = 625 nm and Em = 640 nm), conjugated at specific number and location on DL-DNA branches (Figure 4.1). The ratio of Green (Alexa) and Red (BODIPY) dyes are controlled by the anisotropicity of DNA hybridization, forming barcode populations 4G1R, 2G1R, 1G1R, 1G2R and 1G4R. Detail on this technology can be found in a publication by Li et al. (Li, Cu et al. 2005)

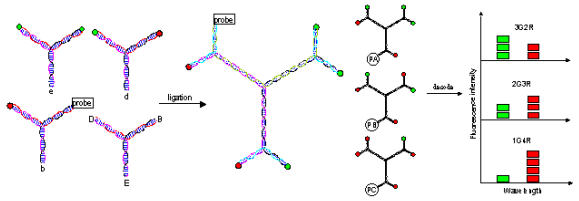

Figure 4.1 Schematic for Construction of Nanobarcodes

The next step to establishing DI-DNA-based nanobarcodes as quantitative biosensing device, it is necessary to characterize its purity, codability and stability. The single nanobarcode (~20nm in diameter) is not visible under conventional fluorescent microscope. To address this problem, populations of each individual nanobarcodes were captured onto 5.5um polystyrene beads for population-based (purity and codability) studies. Capture oligonucleotides conjugated to biotin were immobilized onto avidin-coated polystyrene beads. This entire resulting complex is called the “capture probe”. The target DNA sequence is partially complementary to both capture and report DNA, the latter of which is covalently linked to a fluorescent nanobarcode. In the presence of target DNA, hybridization takes place, and the fluorescent nanobarcode is selectively (by specific sequence hybridization) captured onto the polystyrene beads (Figure 4.2).

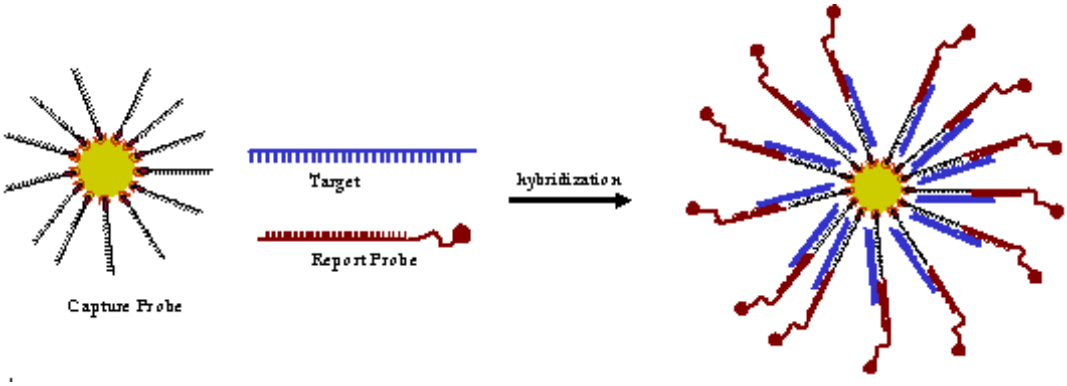

Figure 4.2 Sandwich Hybridization to Polystyrene Beads

The nanobarcode coated beads were visualized using a wide-field and confocal fluorescence microscopy. The fluorescent ratios for green and red emitting dyes for individual beads were recorded and used to assess the purity and coding capability of each population of nanobarcodes.

4.3 Experimental Methods

4.3.1 Setup for Confocal and Wide-field Imaging

The hybridization of nanobarcodes to polystyrene beads via a sandwich assay has been described (Li, Cu et al. 2005). Roughly 2000-3500 beads of each populations, 4G1R, 2G1R, 1G1R, 1G2R, and 1G4R (concentration ~400-700 beads/μl) was deposited separately onto a microscopic glass slide. The beads were allowed to settle onto the bottom of the slide for 10 min, after which 1x volume of 30% glycerol solution was added on top. The samples were covered with a plastic coverslip and allowed to sit at room temperature for an additional 20min.

The beads were visualized under a Olympus BX-50 upright microscope with a mercury arc lamp as excitation source and 100x oil immersion lens (NA = 1.3). Excessive agitation of the slide was avoided, to prevent the beads from staying suspended in solution, which poses a problem when obtaining focus under the microscope. As the lens moves up and down on top of the oil droplet, the slight change in pressure causes any beads in solution to move out of the field of view and focus. Green (Ex = 470/40, Em = 525/50) and red (Ex = 538-582, Em = 613-677) optical filters were applied to measure the fluorescence intensities of each barcode. Separate image acquisition times were used for green and red emissions, and applied to all 5 populations of barcodes. Exposure times were adjusted so that no beads were saturated but still give a discernable signal over the background. For the set of beads discussed in the next section, t_{Green} = 300ms, t_{Red} = 75ms. A neutral filter that blocks ~50% of excitation light was also applied to provide optimum illumination conditions.

4.3.2 Nanobarcode Purity and Decoding

Pictures of in-focus beads were taken as 12-bit *.tif files using MetaMorph (ver. 6.1) software package from Universal Imaging, for both channels (Red and Green), and fluorescent intensities for each beads were collected. The data was processed as an Excel spreadsheet, where the ratio of Red/Green fluorescence for each individual bead was calculated and plotted. The variance was compared to the population mean to assess the population purity. The mean, which represents the “code”, was evaluated to determine the “codability” of the nanobarcodes. In theory, the Red/Green ratio for 1G4R is 4/1 = 4; 1G1R is 1/1 = 1; 4G1R is 1/4 = 0.25, and so on.

The raw R/G ratio of each population was divided, or normalized, by its theoretical R/G (R/G = 1 for 1G1R) to yield an alpha factor value, that is used to normalize raw R/G ratios for all other populations; thus giving 5 alpha factors, which should be similar if the codes are to be used for decoding (only 1 alpha value for the entire set). The alpha factors were compared to evaluate the consistency of the data set—for a consistent data set, the alpha factors for all barcode population must be similar. Statistical t-test was conducted for R/G ratios normalized by one value of alpha factor (1G1R), using empirically determined variance, to confirm that the normalized ratio indeed conforms to the theoretical value, and that the nanobarcodes can be used as a coding device.

The purity of each nanobarcode was assessed by analyzing each population with ANOVA. “Pure” nanobarcode R/G ratios should fall in distinct populations that are significantly different from one another. Pictures of mixture of beads from different population (3, 4, or all 5) were also taken with the same exposure time as the individual beads. The goal is to simulate

"multiplexed detection" of the barcode. Raw R/G ratios calculated from fluorescent net intensities were similarly recorded and analyzed with MS Excel.

4.3.3 Fluorophore Cross-Talking

Beads with only red or green fluorescent dyes were used as control, tGreen = 300ms, tRed = 75ms, with the 50% neutral density filter. Red fluorescence was measured for green dye-conjugated beads, and compared to background value (area without beads) to determine the amount of cross-talking between dyes in each experiment. The fluorescent intensities (A) for each population (N_{Red} = 77, N = 56) was subtracted from the background (B) to yield a net intensity (Z). The standard deviations of each was used to yield a propagated value (dZ), from the formula (dZ/Z)^2 = (dA/A)^2 + (dB/B)^2, where A-B = Z. For samples without cross-talking, the Green fluorescence emission for Red-only conjugated beads must have an average mean of 0, and vice versa. A t-test was applied on population Z with standard deviation dZ, comparing its similarity to a population with mean 0, of the same standard deviation. A confidence interval of 95% was set, and P-value was obtained[4]. A P-value close to 1 indicates that the populations are significantly related (same population), for the conclusion that no cross-talk occurs between the channels (Tables 4.3a, 4.3b).

4.3.4 Nanobarcode Differential Bleaching

In addition, the emission profiles for 1G1R, 1G2R, 1G4R beads (deposited on a glass slide) were also obtained with a fluorescence confocal microscope. The power and gain were adjusted to allow for a clear signal

[4] http://home.clara.net/sisa/t-test.htm

without over-saturation (HV = 750, Gain = 1). Green and red fluorescent intensities were also measured under continuous fluorescent illumination by the confocal microscope for 156s. The extent of bleaching (decrease in bead emission intensities in each channel) was recorded in 100 data points, and used to calculate the bleaching rates, and consequently the differential bleaching (if any) of the barcodes.

4.4 Results

Several sets of data were taken for the analysis of nanobarcode, conducted similarly for proof of reproducibility of the experiment. In the interest of time and brevity, I will focus the result and analysis on only one data set (Barcode092804). Images for red and green fluorescence were taken, and light intensities (in pixels) were recorded for each region (beads). Table 4.1 shows the raw measured R/G ratio, calculated from the ratio of net red and green fluorescent intensities ($I_{net} = I_{bead} – I_{background}$) of each bead, for bead populations 1G4R, 1G2R, 1G1R, 2G1R and 4G1R, with N>60. The alpha factor derived from 1G1R is 1.2, and dividing of the 5 raw R/G ratios by this alpha factor yield “codes” that are close to the theoretical value: 4.02, 2.56, 1, 0.39 and 0.2 for 1G4R → 4G1R respectively (Table 4.1).

Table 4.1 R/G Ratio for 5 Sets of Barcodes and Calculated Alpha Factors

Data Summary (092805)	1G4R	1G2R	1G1R	2G1R	4G1R
Max	6.79	4.74	1.50	3.56	0.28
Min	3.35	2.32	0.93	0.16	0.13
Ave	4.57	2.91	1.14	0.45	0.22
Stdev	0.62	0.42	0.12	0.48	0.03
Count	118.00	108.00	101.00	71.00	64.00
Theoretical	4.00	2.00	1.00	0.50	0.25
Alpha factor 1G4R	**1.14**				
	4.00	2.55	1.00	0.40	0.19
Alpha factor 1G2R		**1.46**			
	3.14	2.00	0.78	0.31	0.15
Alpha factor 1G1R			**1.14**		
	4.02	2.56	1.00	0.40	0.19
Alpha factor 2G1R				**0.91**	
	5.04	3.21	1.26	0.50	0.24
Alpha factor 4G1R					**0.87**
	5.22	3.33	1.30	0.52	0.25

ANOVA test[5] performed on the barcode ratios is yield results, shown on Table 4.2. The F value is 2177, and P-value for the null hypothesis, which assumes that the populations are NOT distinct and is deviated by “chance”, is less than 0.0001. This proves that the barcode ratios are indeed different due to the controlled conjugation of fluorodyes.

Cross-talking between the channels was evaluated by measuring fluorescence emission in red channel for polystyrene beads only conjugated with green dyes, and vice versa. Table 4.3a shows the Red and Green barcode and background intensities for Red-only and Green-only conjugated

[5] http://www.physics.csbsju.edu/stats/anova.html

samples. T-test results for Green fluorescence on Red beads (Red(G)) and Red fluorescence on Green beads (Green(R)), show P-value of 1 for each populations, indicating that there is no significant cross-talking between the channels (Table 4.3b).

Table 4.2 ANOVA Analysis of 5 Barcode Populations

Source of Variation	Sum of Squares	d.f.	Mean Squares	F*
between	1052	4	262.9	2177
error	55.32	458	1208	
total	1107	462		

*The probability of this result, assuming the null hypothesis, is less than .0001. The null hypothesis assumes that the populations are not significantly different.

Table 4.3a Error Propagation of Intensity Background Difference for Red and Green Channels

Bead	Channel	Intensity (A)	Background (B)	dA	dB	(dA/A)^2	(dB/B)^2	Z (A-B)	dZ
Red	R	532	162.7	82.7	6	0.024165	0.0014	369.3	0.1598
(N=77)	G	125.7	122.4	22.4	4.1	0.031756	0.0011	3.3	0.1813
Green	R	161.4	153.1	9.6	16.4	0.003538	0.0115	8.3	0.1225
(N=56)	G	466.1	120.1	72.1	7.4	0.023928	0.0038	346	0.1665

Table 4.3b Calculated P-value for Cross-talking Between Channels

	Red (G)	Green(R)
t-value of Difference	113.8	360
Degree of Freedom	152	110
P-value*	1	1

*The probability of this result, assuming the null hypothesis, is 1.
The nul hypothesis assumes that the populations are not significantly different.

The overlaying of Red and Green fluorescence produces unique barcodes, shown in Figure 4.3. The overlay picture on the right-hand side of Figure 4.3 is the result of overlaying red and green fluorescent signals from Green and Red (on left-hand side); and shows a number of different codes simultaneously on a single slide. The codes 1G4R, 1G2R, 1G1R and 2G1R has overlay color that ranges from red to yellow to green, respectively.

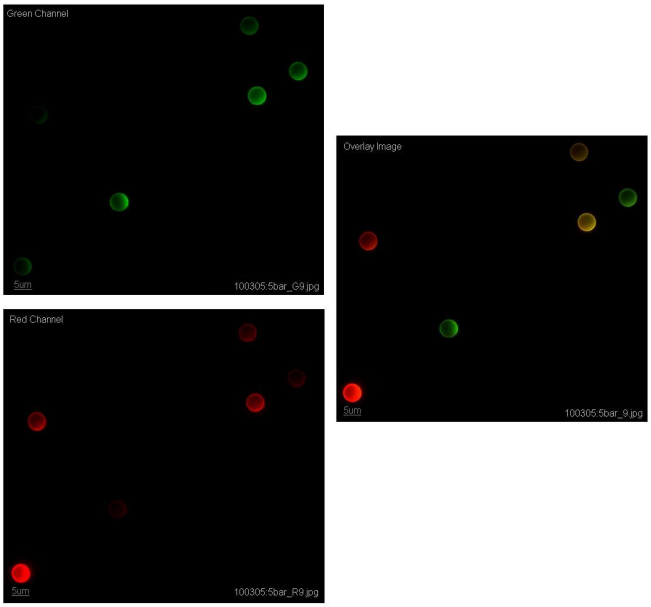

Figure 4.3 Overlay of Red and Green Channels for Pseudo-Color Barcodes

The profiles of 3 codes, 1G4R, 1G2R, and 1G1R shows fluorescent intensities across the bead in a manner as expected (Figure 4.4). Due to the spherical shape of the beads, barcodes in the center are out of focus and does not register lower fluorescence. Note that the inlay pictures are NOT from the same slide that was under the confocal microscope, since some photo bleaching had occurred which prevents them from being reused. Inlay picture on 1G2R is a “crushed” slide, which was created when the objective

lens was brought down too low, and crushed the polystyrene beads between the coverslip and glass slide.

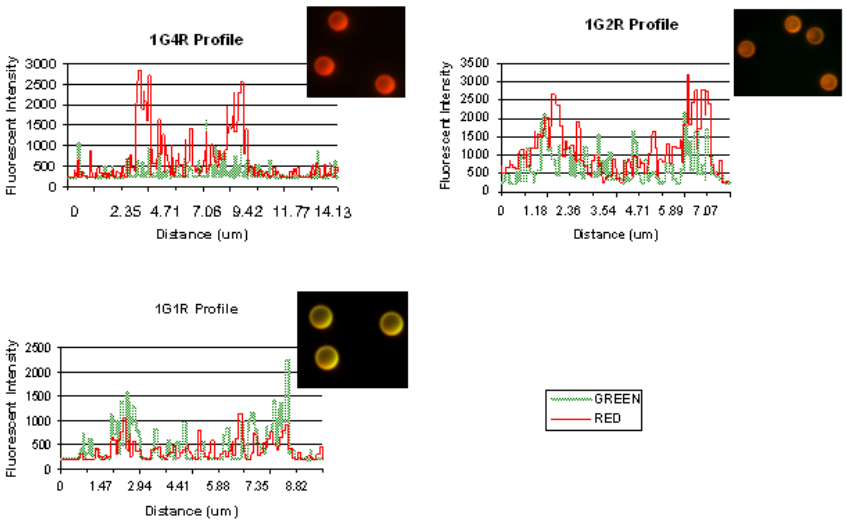

Figure 4.4 Line Profiles Across Beads Of Three Different Barcodes Immobilized On Polystyrene Beads

Figure 4.5 shows fluorescent image of individual beads (polystyrene, d=5.5μm) shows clear difference in bead color, resulted from the precisely controlled ratio of red and green fluorophores conjugated to each barcode. The Green vs. Red (R/G) fluorescent intensity ratios for each beads were obtained and compared against pure populations of five different barcodes (4G1R, 2G1R, 1G1R, 1G2R, 1G4R); subtraction of background fluorescence and a correction factor of 1.2 were also taken into consideration. The decoded results are shown in the table below, where the 7 beads were found to represent 4 different codes: 4G1R, 2G1R, 1G1R, and 1G2R. The exposure times for each bead were: Green = 100ms, Red = 30ms, and the average bead area measure at 3001.6 ± 66.8 pixels.

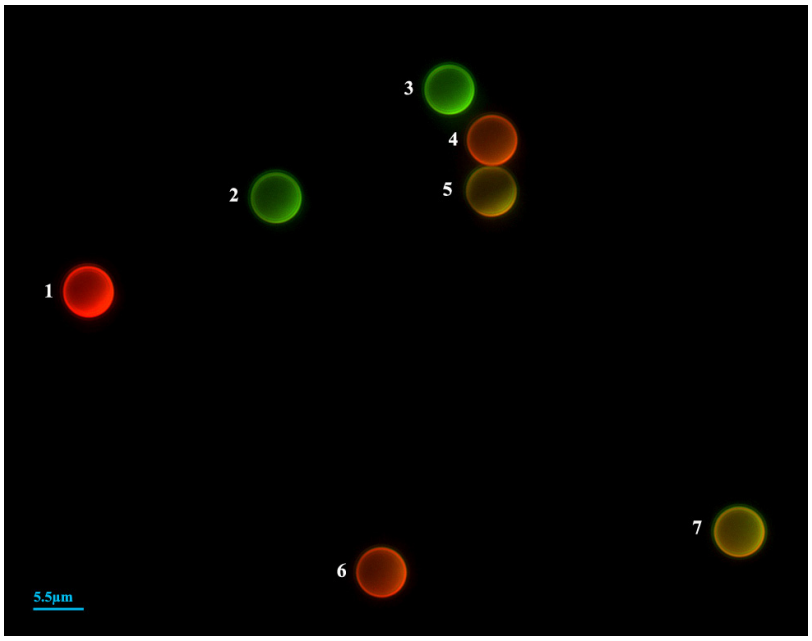

Figure 4.5 Overlay and Simultaneous Decoding of 4 Different Nanobarcodes

Table 4.4 Decoding of Nanobarcodes by R/G Ratio

Bead Number	Corrected R/G Ratio	Decoded Result
1	5.4	1G4R (Ave=3.95 ± 0.48, N=117)
2	0.3	2G1R (Ave=0.34 ± 0.03, N=116)
3	0.3	2G1R
4	2	1G2R (Ave=1.95 ± 0.33, N=61)
5	1	1G1R (Ave=1.00 ± 0.1, N=84)
6	2.4	1G2R
7	1	2G2R

Bleaching of green and red fluorodyes under continuous excitation showed a bleaching rate of 0.21pix/s for Red, and 0.66pix/s for Green dyes (Figure 4.6a, b). The R/G ratio was determined for 4 barcode samples, 4G1R, 1G1R, 1G2R and 1G4R over 2 minutes. The slope of the linear R/G best-fit showed that there is little difference in the R/G ratio after bleaching because the laser power for this experiment was kept at minimum; such that no pixel was oversaturated to obtain proper barcoding ratio, as shown in the bead

profiles (see Figure 4.4). The R^2 values are below 35%, which does not show a good fit. While it may be necessary to prolong the bleaching time to obtain a better fit, the data here also shows that the nanobarcodes is a viable detection device that could be used to follow reactions *in vitro* or *in vivo* for a sufficiently long time.

Table 4.5 Differential Bleaching of Nanobarcodes

Barcode	Sample	R/G Slope (E-5)	R2 (E-2)
4G1R	1	-9	15
	2	-4	4
	3	-5	6
	4	-10	32
1G1R	1	9	0.22
	2	70	32.6
1G2R	1	-50	2.47
1G4R	1	190	2.09
	2	-360	27.8
	3	-40	0.06
	4	-260	7.07
	5	8	0.006

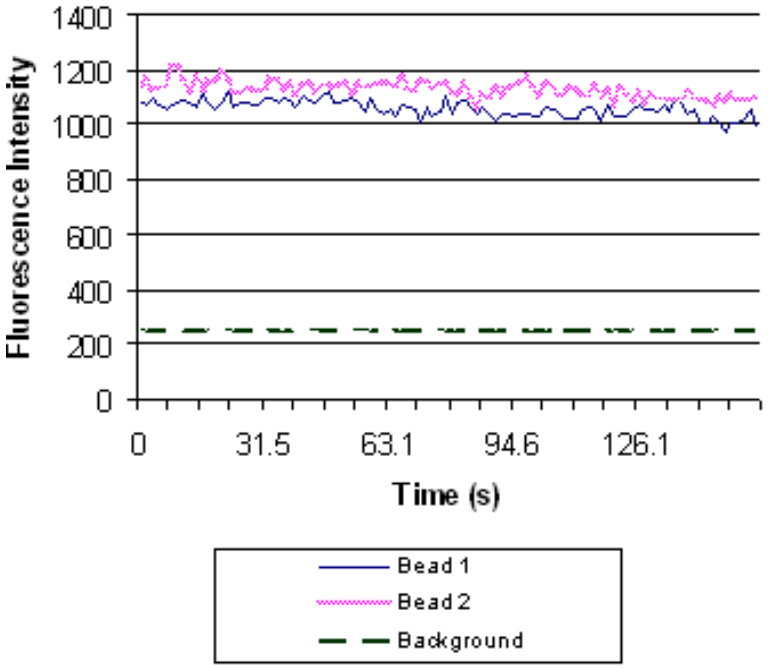

Figure 4.6a Bleaching of Green Fluorodye

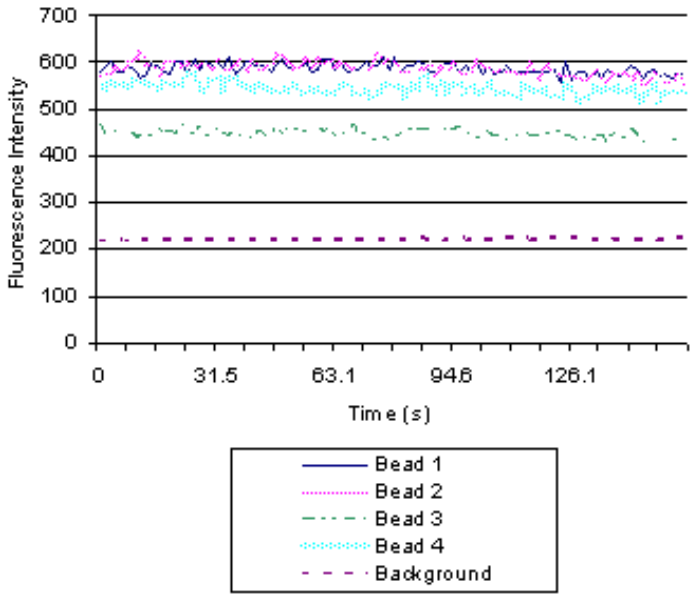

Figure 4.6b Bleaching of Red Fluorodye

4.5 The nanobarcode advantage

In order to verify the important role of DL-DNA in building specific and unique nanobarcodes, a control experiment was run with concentration-based barcodes, where double stranded Red and Green dsDNA were conjugated to polystyrene beads by molar ratios corresponding to that of the DNA nanobarcodes. Similar analysis of this sample (refer to 4.2.1) reveals nonconformity to the expected coding number. (Table 4.6a), as well as a much wider distribution of R/G fluorescence ratio for each barcodes, with 7 times wider distribution range (Table 4.6b). This data is also evidenced on Figure 4.7a where the R/G ratio histograms for all 5 barcodes are plotted, and Figure 4.7b where the same data is plotted as bargraph, to further demonstrate the difference in coding ability and purity of the 2 types of barcodes.

4.6 Conclusion and Discussion

DNA-based fluorescent nanobarcodes have successfully taken advantage of the anisotropic properties of DL-DNA, and was shown by the above analysis to have coding capability, is pure and stable from differential bleaching. Using the nanobarcodes, it is possible to detect multiplexed targets quickly and accurately. The ease in methodology and lack of bulky equipments also is a bonus, when working in the field. The DNA nanobarcode is a versatile and convenient device, though not without disadvantages. The thermo and pH sensitive property, and susceptibility to enzyme degradation of dsDNA is a limiting factor in terms of working environment. Also, the size of nanobarcodes may be too small, and thus be difficult to resolve the actual target. Though the concept of DL-DNA based fluorescent nanobarcode has been actualized, further study is needed to bring it to real-world application.

Table 4.6a R/G Ratio for DNA Nanobarcodes and Calculated Alpha Factors

Data Summary (022705)	1G4R	1G2R	1G1R	2G1R	4G1R
Max	19.80	20.37	6.95	2.53	1.77
Min	5.66	2.98	1.92	0.70	0.30
Ave	**9.87**	**7.31**	**4.07**	**1.44**	**0.66**
Stdev	**3.61**	**3.86**	**1.46**	**0.54**	**0.31**
Count	29.00	49.00	40.00	22.00	34.00
Theoretical	4.00	2.00	1.00	0.50	0.25
Alpha factor 1G4R	**2.47**				
	4.00	2.96	1.65	0.58	0.27
Alpha factor 1G2R		**3.65**			
	2.70	2.00	1.11	0.40	0.18
Alpha factor 1G1R			**4.07**		
	2.42	1.79	1.00	0.35	0.16
Alpha factor 2G1R				**2.89**	
	3.42	2.53	1.41	0.50	0.23
Alpha factor 4G1R					**2.65**
	3.72	2.75	1.54	0.54	0.25

Table 4.6b Variance Comparison for Concentration-Based and DNA Nanobarcodes

22705	Concentration-Based Barcode	STDEV		DNA Nanobarcode	STDEV	
1G4R	2.42	0.89	0.37	4.02	0.54	0.14
1G2R	1.79	0.95	0.53	2.50	0.27	0.11
1G1R	1.00	0.36	0.36	1.00	0.10	0.10
2G1R	0.35	0.13	0.37	0.30	0.08	0.27
4G1R	0.16	0.08	0.47	0.19	0.03	0.14

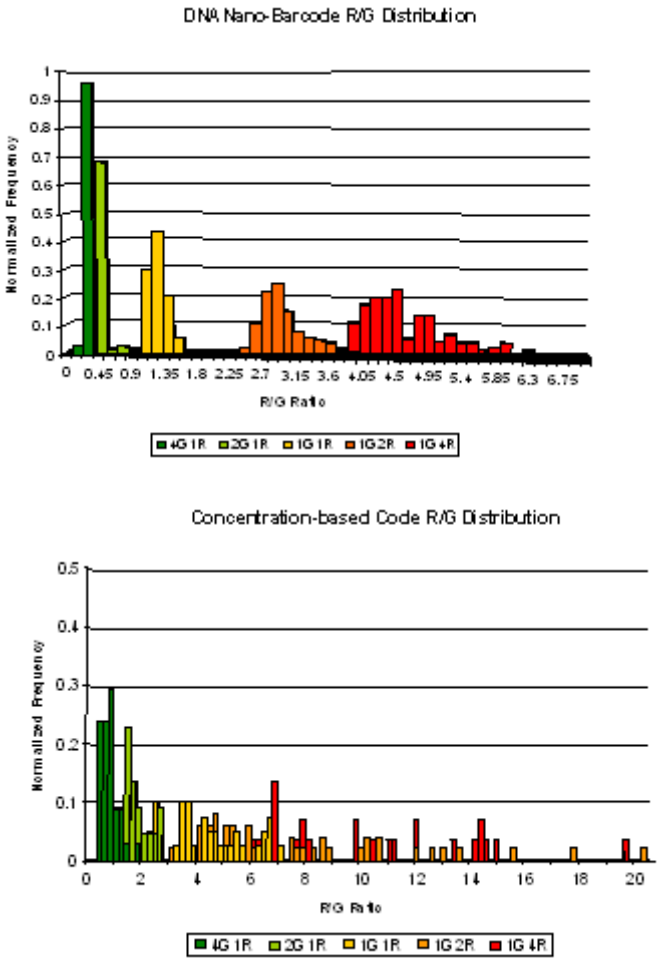

Figure 4.7a R/G Ratio Distribution for DNA Nanobarcode and Concentration-Based Barcodes

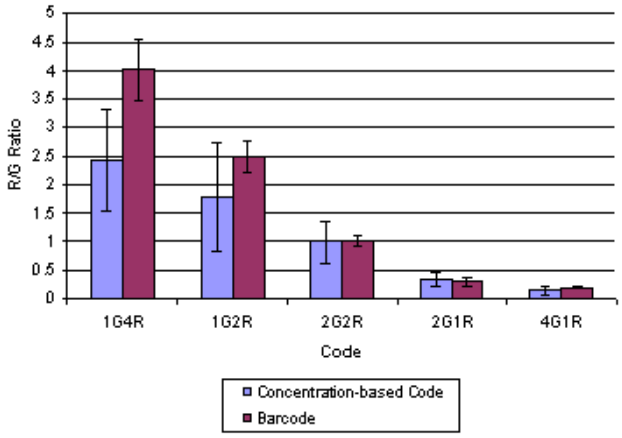

Figure 4.7b Comparison for Concentration-Based vs. DNA Nanobarcode

REFERENCES

Adleman, L. M. (1994). "Molecular computation of solutions to combinatorial problems." Science **266**(5187): 1021-4.

Allemand, J. F., D. Bensimon, et al. (1998). "Stretched and overwound DNA forms a Pauling-like structure with exposed bases." Proc Natl Acad Sci U S A **95**(24): 14152-7.

Bloomfield, V. A., Crothers, D. M., Tinoco, I. (2000). Nucleic Acids: Structures, Properties, and Functions. Sausalito, University Science Books.

Braun, E., Y. Eichen, et al. (1998). "DNA-templated assembly and electrode attachment of a conducting silver wire." Nature **391**(6669): 775-8.

Broude, N. E. (2002). "Stem-loop oligonucleotides: a robust tool for molecular biology and biotechnology." Trends Biotechnol **20**(6): 249-56.

Bustamante, C., Z. Bryant, et al. (2003). "Ten years of tension: single-molecule DNA mechanics." Nature **421**(6921): 423-7.

Chan, W. C. and S. Nie (1998). "Quantum dot bioconjugates for ultrasensitive nonisotopic detection." Science **281**(5385): 2016-8.

Chaput, J. C. and J. W. Szostak (2003). "TNA synthesis by DNA polymerases." J Am Chem Soc **125**(31): 9274-5.

Chen, J. H. and N. C. Seeman (1991). "Synthesis from DNA of a molecule with the connectivity of a cube." Nature **350**(6319): 631-3.

Critchlow, S. E., O'Dea, M. H., Howells, A. J., Couturier, M., Gellert, M. and Maxwell, A. (1997). "The Interaction of the F Plasmid Killer Protein, CcdB, with DNA Gyrase: Induction of DNA Cleavage and Blocking of Transcription." J. Mol. Biol. **273**: 826-839.

Ding, B., R. Sha, et al. (2004). "Pseudohexagonal 2D DNA crystals from double crossover cohesion." J Am Chem Soc **126**(33): 10230-1.

Elghanian, R., J. J. Storhoff, et al. (1997). "Selective colorimetric detection of polynucleotides based on the distance-dependent optical properties of gold nanoparticles." Science **277**(5329): 1078-81.

Endo, M., T. Hayashi, et al. (2004). "Applications of carbon nanotubes in the twenty-first century." Philos Transact A Math Phys Eng Sci **362**(1823): 2223-38.

Essevaz-Roulet, B., U. Bockelmann, et al. (1997). "Mechanical separation of the complementary strands of DNA." Proc Natl Acad Sci U S A **94**(22): 11935-40.

Fu, A., C. M. Micheel, et al. (2004). "Discrete nanostructures of quantum dots/Au with DNA." J Am Chem Soc **126**(35): 10832-3.

Fu, T. J. and N. C. Seeman (1993). "DNA double-crossover molecules." Biochemistry **32**(13): 3211-20.

He, P. and L. Dai (2004). "Aligned carbon nanotube-DNA electrochemical sensors." Chem Commun (Camb)(3): 348-9.

.

Kallenbach, N. R., Ma, R.I. & Seeman, N.C. (1983). "An Immobile Nucleic-Acid Junction Constructed from Oligonucleotides." Nature(305): 829-831.

Keren, K., R. S. Berman, et al. (2003). "DNA-templated carbon nanotube field-effect transistor." Science **302**(5649): 1380-2

Keren, K., M. Krueger, et al. (2002). "Sequence-specific molecular lithography on single DNA molecules." Science **297**(5578): 72-5.

LaBean, T. H. Y., H.; Kopatsch, J.; Liu, F. R.; Winfree, E.; Reif, J. H.; Seeman, N. C. (2000). "Construction, analysis, ligation, and self-assembly of DNA triple crossover complexes." J. Am. Chem. Soc(122): 1848-1860.

Li, S., P. He, et al. (2005). "DNA-directed self-assembling of carbon nanotubes." J Am Chem Soc **127**(1): 14-5.

Li, Y., Y. T. Cu, et al. (2005). "Multiplexed detection of pathogen DNA with DNA-based fluorescence nanobarcodes." Nat Biotechnol.

Li, Y., Y. D. Tseng, et al. (2004). "Controlled assembly of dendrimer-like DNA." Nat Mater **3**(1): 38-42.

Liu, D., S. H. Park, et al. (2004). "DNA nanotubes self-assembled from triple-crossover tiles as templates for conductive nanowires." Proc Natl Acad Sci U S A **101**(3): 717-22.

Liu, H., J. Gao, et al. (2003). "A four-base paired genetic helix with expanded size." Science **302**(5646): 868-71.

Lukeman, P. S., A. C. Mittal, et al. (2004). "Two dimensional PNA/DNA arrays: estimating the helicity of unusual nucleic acid polymers." Chem Commun (Camb)(15): 1694-5.

Luo, D. (2003). "The road from biology to materials." Materials Today: 38-43.

Ma, R. I., N. R. Kallenbach, et al. (1986). "Three-arm nucleic acid junctions are flexible." Nucleic Acids Res **14**(24): 9745-53.

Mao, C., T. H. LaBean, et al. (2000). "Logical computation using algorithmic self-assembly of DNA triple-crossover molecules." Nature **407**(6803): 493-6.

Mao, C., W. Sun, et al. (1997). "Assembly of Borromean rings from DNA." Nature **386**(6621): 137-8.

Mao, C., Sun, W., Seeman, N. C. (1999). "Designed Two-Dimensional DNA Holliday Junction Arrays Visualized by Atomic Force Microscopy." J. Am. Chem. Soc **121**: 5437-5443.

Mao, C., Sun, W., Shen, Z. & Seeman, N.C. (1999). "A nanomechanical device based on the B-Z transition of DNA." Nature(397): 144-146.

Mathieu, F., S. Liao, et al. (2005). "Six-helix bundles designed from DNA." Nano Lett **5**(4): 661-5.

Medintz, I. L., H. T. Uyeda, et al. (2005). "Quantum dot bioconjugates for imaging, labelling and sensing." Nat Mater **4**(6): 435-46.

Mirkin, C. A. (2000). "Programming the assembly of two- and three-dimensional architectures with DNA and nanoscale inorganic building blocks." Inorg Chem **39**(11): 2258-72.

Mizuuchi, K., Mizuuchi, M., Gellert, M. (1982). "Cruciform Structures in Palindromic DNA are Favored by DNA supercoiling." J. Mol. Biol. **156**: 229-243.

Mucic, R. C., Storhoff, J. J., Mirkin, C. A., Letsinger, R. L. (1998). "Directed Synthesis of Binary Nanoparticle Network Materials." Journal of the American Chemical Society **120**: 12674-12675.

Nam, J. M., S. I. Stoeva, et al. (2004). "Bio-bar-code-based DNA detection with PCR-like sensitivity." J Am Chem Soc **126**(19): 5932-3.

Nelson, D. L. C., M. M. (2000). Lehninger Principles of Biochemistry. New York, W H Freeman & Co.

Niemeyer, C. (1999). "Progress in "engineering up" nanotechnology devices utilizing DNA as a construction material." Appl. Phys. A Matls. Sci. & Proc.(68): 119-124.

Rosi, N. L., C. S. Thaxton, et al. (2004). "Control of nanoparticle assembly by using DNA-modified diatom templates." Angew Chem Int Ed Engl **43**(41): 5500-3.

Sa-Ardyen, P., N. Jonoska, et al. (2004). "Self-assembly of irregular graphs whose edges are DNA helix axes." J Am Chem Soc **126**(21): 6648-57.

Sa-Ardyen, P., A. V. Vologodskii, et al. (2003). "The flexibility of DNA double crossover molecules." Biophys J **84**(6): 3829-37.

SantaLucia, J., Jr. (1998). "A unified view of polymer, dumbbell, and oligonucleotide DNA nearest-neighbor thermodynamics." Proc Natl Acad Sci U S A **95**(4): 1460-5.

Seeman, N. C. (1982). "Nucleic acid junctions and lattices." J Theor Biol **99**(2): 237-47.

Seeman, N. C. (1990). "De novo design of sequences for nucleic acid structural engineering." J Biomol Struct Dyn **8**(3): 573-81.

Seeman, N. C. (1998). "DNA Nanotechnology: Novel DNA Constructions." Annu Rev Biophys Biomol Struct **27**: 225-48.

Seeman, N. C. (2003). "At the crossroads of chemistry, biology, and materials: structural DNA nanotechnology." Chem Biol **10**(12): 1151-9.

Seeman, N. C. (2005). "From genes to machines: DNA nanomechanical devices." Trends Biochem Sci **30**(3): 119-25.

Seeman, N. C. (2005). "Structural DNA nanotechnology: an overview." Methods Mol Biol **303**: 143-66.

Sha, R., F. Liu, et al. (2000). "Atomic force microscopy of parallel DNA branched junction arrays." Chem Biol **7**(9): 743-51.

Shih, W. M., J. D. Quispe, et al. (2004). "A 1.7-kilobase single-stranded DNA that folds into a nanoscale octahedron." Nature **427**(6975): 618-21.

Simmel, F. C., B. Yurke, et al. (2002). "Operation kinetics of a DNA-based molecular switch." J Nanosci Nanotechnol **2**(3-4): 383-90.

Simmel, F. C. Y., B. (2002). "A DNA-based molecular device switchable between three distinct mechanical states." Appl Phys Lett(80): 883-885.

Smith-Keary, P. F. (1989). Molecular Genetics of Escherichia coli. New York, The Guilford Press.

Stavis, S. M., J. B. Edel, et al (2005) "Detection and Identification of Nucleic Acid Engineered Fluorescent Labels in Submicrometre Fluidic Channels", Nanotechnology, **16**, S314-S323.

Stojanovic, M. N. and D. Stefanovic (2003). "A deoxyribozyme-based molecular automaton." Nat Biotechnol **21**(9): 1069-74.

Strick, T. R., J. F. Allemand, et al. (2000). "Stress-induced structural transitions in DNA and proteins." Annu Rev Biophys Biomol Struct **29**: 523-43.

Wang, Y. L., J. E. Mueller, et al. (1991). "Assembly and characterization of five-arm and six-arm DNA branched junctions." Biochemistry **30**(23): 5667-74.

Whitesides, G. M., J. P. Mathias, et al. (1991). "Molecular self-assembly and nanochemistry: a chemical strategy for the synthesis of nanostructures." Science **254**(5036): 1312-9.

Williams, L. D. and L. J. Maher, 3rd (2000). "Electrostatic mechanisms of DNA deformation." Annu Rev Biophys Biomol Struct **29**: 497-521.

Winfree, E., F. Liu, et al. (1998). "Design and self-assembly of two-dimensional DNA crystals." Nature **394**(6693): 539-44.

Yan, H., Park, S. H., Finkelstein, G., Reif, J. H., and LaBean, T. H. (2003). "DNA-Templated Self-Assembly of Protein Arrays and Highly Conductive Nanowires." Science **301**: 1882-86.

Yan, H., X. Zhang, et al. (2002). "A robust DNA mechanical device controlled by hybridization topology." Nature **415**(6867): 62-5.

Yoshina-Ishii, C. and S. G. Boxer (2003). "Arrays of mobile tethered vesicles on supported lipid bilayers." J Am Chem Soc **125**(13): 3696-7.

Zhang, S. (2003). "Fabrication of novel biomaterials through molecular self-assembly." Nat Biotechnol **21**(10): 1171-8.

Zheng, M., A. Jagota, et al. (2003). "Structure-based carbon nanotube sorting by sequence-dependent DNA assembly." Science **302**(5650): 1545-8.

Zhu, L., P. S. Lukeman, et al. (2003). "Nylon/DNA: Single-stranded DNA with a covalently stitched nylon lining." J Am Chem Soc **125**(34): 10178-9.